

spectra for vagal stimulation  $[N(f)]$  and HR  $[HR(f)]$  [16]. Over the eight segments, the power of the vagal stimulation  $[S_{N,N}(f)]$ , the power of the HR  $[S_{HR,HR}(f)]$ , and the cross-power between these two signals  $[S_{N,HR}(f)]$  were ensemble averaged. Lastly, the transfer function  $[H(f)]$  from vagal stimulation to the HR response was estimated as follows [17, 18].

$$[H(f)] = \frac{S_{N,HR}(f)}{S_{N,N}(f)} \quad (1)$$

In previous studies [6, 14] the transfer function from vagal stimulation to HR response approximated a first-order, low-pass filter with a lag time; therefore the estimated transfer function was parameterized using the following mathematical model.

$$H(f) = \frac{-K}{1 + \frac{f}{fc} j} e^{-2\pi f L} \quad (2)$$

where  $K$  represents the dynamic gain (or, to be more accurate, the steady-state gain, in  $\text{beats} \cdot \text{min}^{-1} \cdot \text{Hz}^{-1}$ ),  $fc$  denotes the corner frequency (in Hz),  $L$  denotes the lag time (in s), and  $f$  and  $j$  represent frequency and imaginary unit, respectively. The negative sign in the numerator indicates the negative HR response to vagal stimulation. The steady-state gain indicates the asymptotic value of the relative amplitude of HR response to vagal nerve stimulation when the frequency of input modulation approaches zero. The corner frequency represents the frequency of input modulation at which gain decreases by 3 dB from the steady-state gain in the frequency domain. The corner frequency reflects the rapidity of the HR response to vagal stimulation; the higher the corner frequency, the faster the HR response. The dynamic gain, corner frequency, and lag time were estimated by means of an iterative nonlinear least-squares regression. The phase shift of the transfer function indicates, with respect to the input signal, a lag or lead in the output signal normalized by its corresponding frequency of input modulation.

To quantify the linear dependence of the HR response on vagal stimulation, the magnitude-squared coherence function  $[\text{Coh}(f)]$  was estimated as follows [17, 18].

$$[\text{Coh}(f)] = \frac{|S_{N,HR}(f)|^2}{S_{N,N}(f) \cdot S_{HR,HR}(f)} \quad (3)$$

Coherence values range from zero to unity. Unity coherence indicates perfect linear dependence between the input signals and output signals; in contrast, zero coherence indicates total independence between the two.

To facilitate the intuitive understanding of the system dynamic characteristics, we calculated the system step response of HR to 1 Hz nerve stimulation as follows. The system impulse response was derived from the inverse Fourier transform of  $H(f)$ . The system step response was then obtained from the time integral of the impulse response. The length of the step response was 51.2 s. We calculated the maximum step response by averaging the

last 10 s of the step response. The time constant of the step response was calculated from the corner frequency of the corresponding transfer function using the following relationship.

$$\text{Time constant} = \frac{1}{2 \cdot \pi \cdot fc} \quad (4)$$

In this definition, the time constant is related inversely to the corner frequency without being influenced by the lag time.

The static transfer function from stepwise vagal stimulation to HR was estimated by averaging the HR data during the final 10 s of the 60 s stimulation at each stimulation step.

**Statistical analysis.** Values are mean  $\pm$  SD. A two-way ANOVA, with drug and CSS as the main effects, was used to test the differences among parameters.  $P < 0.05$  was considered significant.

## RESULTS

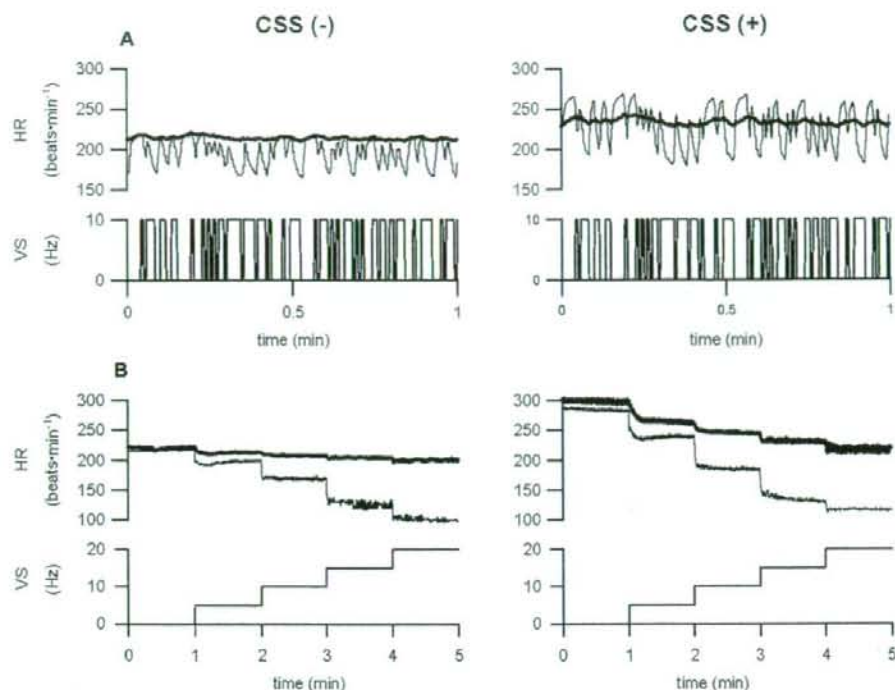
Figure 1A shows recordings typical of the dynamic protocol. The top panels show HR under conditions of control (thin lines) and  $K_{ACh}$  channel blockade (thick lines), without (left) and with (right) CSS. The bottom panels show the binary white-noise signal used for vagal stimulation. Random vagal stimulation decreased HR intermittently. Tertiapin attenuated the HR variation in response to the dynamic vagal stimulation. CSS increased the mean level of HR and augmented HR variation in response to the dynamic vagal stimulation.

Figure 1B shows recordings typical of the static protocol. The top panels illustrate HR under conditions of control (thin lines) and  $K_{ACh}$  channel blockade (thick lines), without (left) and with (right) CSS. The bottom panels depict the vagal stimulation frequency. The stepwise vagal stimulation decreased HR in a stepwise manner. Tertiapin attenuated the bradycardic response to vagal stimulation regardless of CSS, which increased baseline HR and contributed to augment the response.

### Dynamic protocol

The mean values of AP and HR before and during dynamic vagal stimulation are summarized in Table 1. This stimulation did not affect AP under any of the conditions, but it significantly decreased the mean HR except under the conditions of  $K_{ACh}$  channel blockade without CSS, which increased the mean HR ( $P < 0.01$ ), but not the mean AP, both before and during vagal stimulation.

Figure 2A illustrates the dynamic transfer functions characterizing the vagal HR control averaged for all animals under conditions of control (thin lines) and  $K_{ACh}$  channel blockade (thick lines), without (left) and with (right) CSS. Gain plots, phase plots, and coherence functions are shown. Note that the frequency axes of these plots indicate the modulation frequency of the random



**Fig. 1. A:** Representative recordings of HR obtained utilizing binary white-noise vagal stimulation (top) and the corresponding vagal stimulation (VS; bottom) without (left) and with (right) CSS. Thin line, control; thick line,  $K_{ACh}$  channel blockade with tertipin ( $30 \text{ nmol}\cdot\text{kg}^{-1}$  iv). **B:** Representative recordings of HR obtained utilizing stepwise vagal stimulation (top) and the corresponding VS (bottom) without (left) and with (right) CSS, which increased the basal HR and the amplitude of HR variation in both binary white-noise and stepwise vagal stimulations. A  $K_{ACh}$  channel blockade attenuated the amplitude of HR variation and the speed of the response of HR to vagal stimulation regardless of CSS.

**Table 1.** Effects of tertipin infusion and CSS on AP and HR before and during dynamic vagal stimulation.

	CSS (-)		CSS (+)		Comparison factors		
	Control	Tertipin	Control	Tertipin	Drug	CSS	Interaction
AP, mmHg							
Before stimulation	82.2 ± 16.8	76.7 ± 20.1	90.5 ± 13.8	81.8 ± 16.6	0.022	0.641	0.546
During stimulation	80.2 ± 18.4	76.6 ± 21.4	81.8 ± 14.8	75.9 ± 19.0	0.144	0.962	0.709
HR, beats·min <sup>-1</sup>							
Before stimulation	247.8 ± 20.1	247.9 ± 30.8	312.2 ± 15.6	307.4 ± 20.9	0.521	<0.001	0.494
During stimulation	211.9 ± 17.5**	228.3 ± 23.4	244.3 ± 33.3**	248.1 ± 30.7**	0.026	<0.001	0.308

Values are means ± SD ( $n = 7$ ). CSS, cardiac sympathetic stimulation; AP, arterial pressure; HR, heart rate. \*\* $P < 0.01$  vs. corresponding values before stimulation. Tertipin was infused at  $30 \text{ nmol/kg}$  iv.

input signal and not the vagal stimulation frequency itself. Table 2 summarizes parameters of the transfer function at 0.01, 0.1, 0.5, and 1 Hz and also those of the step response. Tertipin attenuated the dynamic gain compared with the control conditions regardless of CSS. The phase approached  $-\pi$  radians at the lowest frequency and lagged with increasing frequency under the control conditions. Tertipin increased the phase delay in the

frequency range from 0.01 to 1 Hz. Coherence was near unity in the overall frequency range under the control conditions. A decrease in the coherence function from unity was noted  $>0.6$  Hz under the condition of the  $K_{ACh}$  channel blockade, which was reversed by CSS.

Figure 2B shows the calculated step response of HR to vagal stimulation averaged for all animals under the conditions of control (thin lines) and  $K_{ACh}$  channel blockade

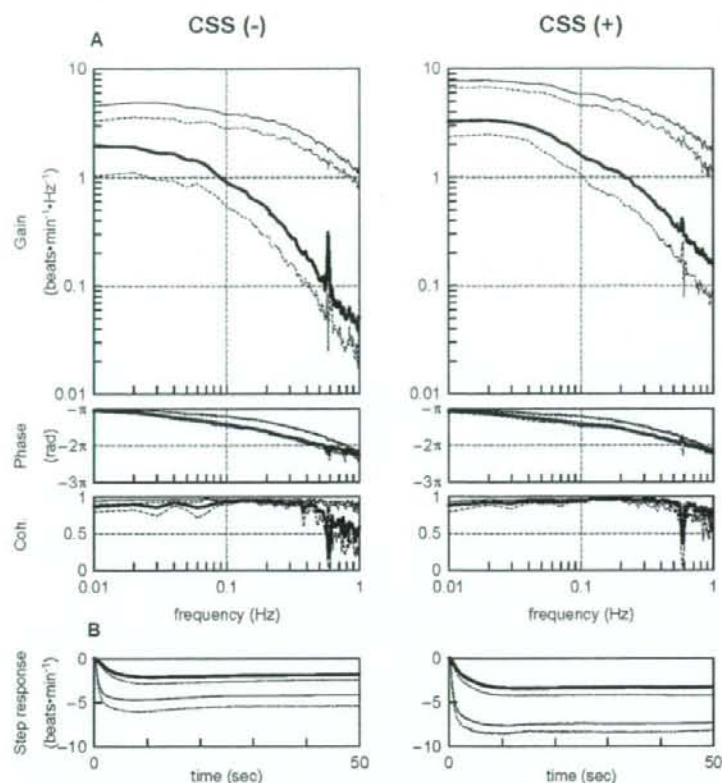


**Fig. 2. A:** Dynamic transfer function relating vagal stimulation to the HR responses averaged from all animals (pooled data;  $n = 7$ ) without (left) and with (right) CSS. Solid lines, means; dashed lines,  $-SD$ . Thin line, control; thick line, a  $K_{ACh}$  channel blockade with tertipin ( $30 \text{ nmol}\cdot\text{kg}^{-1} \text{ iv}$ ). Top: gains; middle: phase shifts; bottom: coherence (Coh) functions. Tertipin decreased transfer gain and increased the phase shift with increasing frequency. Cardiac sympathetic stimulation increased transfer gain both under control conditions and under conditions of a  $K_{ACh}$  channel blockade without affecting the phase shift. **B:** Calculated step response to 1 Hz tonic vagal stimulation averaged from all animals (pooled data;  $n = 7$ ) without (left) and with (right) CSS. Solid lines, means; dashed lines,  $-SD$ . Thin line, control; thick line,  $K_{ACh}$  channel blockade with tertipin ( $30 \text{ nmol}\cdot\text{kg}^{-1} \text{ iv}$ ). The  $K_{ACh}$  channel blockade decreased the maximum step response and slowed the initial step response. CSS increased the maximum step response both under control conditions and under conditions of a  $K_{ACh}$  channel blockade without affecting the initial response (see Table 2).

**Table 2.** Effects of tertipin infusion and CSS on parameters of the transfer function and step response.

	CSS (-)		CSS (+)		Comparison factors		
	Control	Tertipin	Control	Tertipin	Drug	CSS	Interaction
Gain, beats·min <sup>-1</sup> ·Hz <sup>-1</sup>							
0.01 Hz	4.58 ± 1.26	2.21 ± 0.97	7.73 ± 1.15	3.28 ± 0.92	<0.001	0.001	0.007
0.1 Hz	3.81 ± 1.01	1.10 ± 0.43	5.82 ± 1.28	1.60 ± 0.54	<0.001	0.007	0.015
0.5 Hz	2.12 ± 0.64	0.16 ± 0.07	3.08 ± 0.82	0.36 ± 0.17	<0.001	0.013	0.081
1 Hz	1.09 ± 0.27	0.08 ± 0.03	1.73 ± 0.61	0.16 ± 0.08	<0.001	0.019	0.044
Phase, rad							
0.01 Hz	3.10 ± 0.04	2.99 ± 0.11	2.99 ± 0.11	2.92 ± 0.14	0.037	0.077	0.579
0.1 Hz	2.52 ± 0.08	1.78 ± 0.17	2.52 ± 0.11	1.83 ± 0.25	<0.001	0.757	0.719
0.5 Hz	0.91 ± 0.13	0.03 ± 0.27	0.90 ± 0.10	0.35 ± 0.10	<0.001	0.011	0.056
1 Hz	-0.56 ± 0.33	-0.81 ± 0.21	-0.41 ± 0.26	-0.64 ± 0.18	0.014	0.159	0.905
Coherence							
0.01 Hz	0.95 ± 0.05	0.87 ± 0.07	0.93 ± 0.04	0.89 ± 0.09	0.005	0.947	0.424
0.1 Hz	0.96 ± 0.03	0.94 ± 0.04	0.97 ± 0.01	0.95 ± 0.02	0.004	0.440	0.835
0.5 Hz	0.96 ± 0.02	0.83 ± 0.08	0.91 ± 0.08	0.93 ± 0.04	0.026	0.259	0.006
1 Hz	0.90 ± 0.07	0.59 ± 0.16	0.78 ± 0.15	0.79 ± 0.12	0.017	0.312	0.011
Maximum step response, beats·min <sup>-1</sup>	-4.2 ± 1.2	-1.8 ± 0.6	-7.4 ± 0.9	-3.3 ± 0.9	<0.001	<0.001	0.005
Time constant, s	0.63 ± 0.09	3.34 ± 0.55	0.74 ± 0.18	3.18 ± 1.10	<0.001	0.913	0.560

Values are means ± SD ( $n = 7$ ). CSS, cardiac sympathetic stimulation. Tertipin was infused at  $30 \text{ nmol}/\text{kg} \text{ iv}$ .

**Table 3.** Effects of tertiapin infusion and CSS on parameters of the transfer function relating dynamic vagal stimulation to HR.

	CSS (-)		CSS (+)		Comparison factors		
	Control	Tertiapin	Control	Tertiapin	Drug	CSS	Interaction
Dynamic gain, beats·min <sup>-1</sup> ·Hz <sup>-1</sup>	4.6 ± 1.1	2.3 ± 0.9	7.3 ± 1.1	3.6 ± 1.0	<0.001	<0.001	0.037
Corner frequency, Hz	0.26 ± 0.04	0.05 ± 0.01	0.23 ± 0.06	0.06 ± 0.02	<0.001	0.439	0.1613
Lag time, s	0.38 ± 0.04	0.45 ± 0.04	0.34 ± 0.04	0.38 ± 0.03	<0.001	0.002	0.2776

Values are means ± SD (*n* = 7). CSS, cardiac sympathetic stimulation; HR, heart rate. Tertiapin was infused at 30 nmol/kg iv.

(thick lines), without (left) and with (right) CSS. Tertiapin slowed the transient response and attenuated the HR response to vagal stimulation in the time domain. CSS did not affect the time constant, though it augmented the maximum step response. A significant interaction was observed between the tertiapin and CSS effects in the maximum step response, but not in the time constant (Table 2).

The fitted parameters of the transfer functions are summarized in Table 3. Tertiapin significantly decreased the dynamic gain and the corner frequency and significantly increased the lag time. Conversely, CSS significantly increased the dynamic gain and significantly decreased the lag time. A significant interaction was observed between the tertiapin and CSS effects only in dynamic gain.

#### Static protocol

Figure 3A summarizes changes in HR in response to stepwise vagal stimulation without (left) and with (right) CSS, which increased basal HR obtained at 0 Hz vagal stimulation by approximately 50 beats·min<sup>-1</sup>. Tertiapin significantly attenuated the bradycardic response to vagal stimulation regardless of CSS. The magnitude of attenuation (i.e., the difference between the open and closed symbols) became greater as the vagal stimulation frequency increased.

Figure 3B demonstrates the HR reduction obtained under four conditions at each frequency. To aid an intuitive understanding, the tertiapin condition is designated as D(-) in this panel because tertiapin blocked the direct action of ACh. S(+) indicates the presence of CSS. At 5 Hz vagal stimulation frequency, the direct action alone S(-)D(+) significantly augmented the HR reduction, as depicted by the diagonal hatch. CSS alone S(+D(-) also significantly augmented the HR reduction, as depicted by the vertical hatch. The augmentation of the HR reduction obtained by S(+D(+) exceeded the simple summation of the diagonal hatch and vertical hatch, suggesting that the effect of the direct action was enhanced by CSS (depicted in the solid rectangle). The positive interaction waned at 10 Hz vagal stimulation and disappeared at 15 and 20 Hz vagal stimulation. That is, the simple summation of the

diagonal hatch and vertical hatch largely explained the augmentation of the HR reduction attained by S(+D(+) at 15 and 20 Hz vagal stimulation.

#### DISCUSSION

We have examined the effect of background sympathetic tone on the direct action of ACh through  $K_{ACh}$  channels by examining the dynamic and static transfer characteristics. The major findings in the present study are that the bradycardic response to vagal stimulation via the  $K_{ACh}$  channels was augmented by concomitant CSS, depending on vagal stimulation frequency. The rapidity of vagal HR control obtained by the  $K_{ACh}$  channels, however, was not affected by CSS. These findings support our hypotheses and demonstrated, for the first time to our knowledge, the existence of an accentuated antagonism in the direct action of ACh through the  $K_{ACh}$  channels.

#### Effect of CSS on the rapidity of vagal HR control via $K_{ACh}$ channels

Our results indicate that the rapidity of the vagal HR control via the  $K_{ACh}$  channels was not affected by background sympathetic tone. In the transfer function, the phase values were significantly more delayed by the  $K_{ACh}$  channel blockade in the frequency range from 0.01 to 1 Hz in agreement with our previous study [6]. In contrast, CSS did not affect the phase characteristics, in which no significant interaction was observed at each frequency (Table 2). Moreover, the calculated step response clearly demonstrated that tertiapin significantly prolonged the time constant by >2 s, whereas CSS did not affect it (Fig. 2B and Table 2).

Changes in fitted parameters of the transfer function from vagal stimulation to HR also support our first hypothesis that CSS does not affect the rapidity of the vagal HR control mediated by the  $K_{ACh}$  channels. Tertiapin decreased the corner frequency to a similar degree without or with CSS, which did not affect the corner frequency. On the other hand, tertiapin prolonged the lag time, whereas CSS shortened it (Table 3). However, changes in the lag time caused by tertiapin or CSS were less than 0.1 s and might

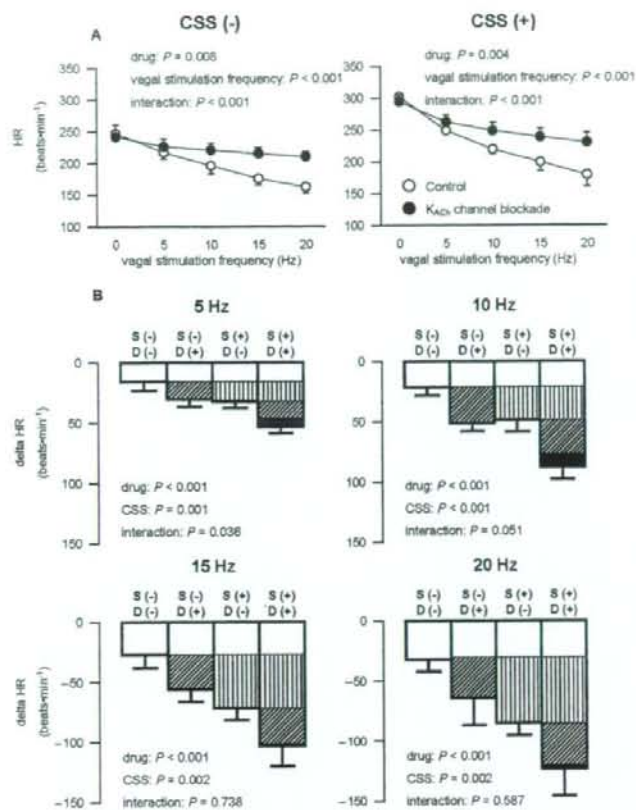


**Fig. 3. A:** Static HR responses relating stepwise vagal stimulation averaged from all animals (pooled data;  $n = 5$ ) without (left) and with (right) CSS. A  $K_{ACh}$  channel blockade decreases the static HR response, and the static reductions in the bradycardic effect were greater at higher stimulation frequencies in both conditions. **B:** Changes in HR responses from baseline to vagal stimulation at 5 Hz (top left), 10 Hz (top right), 15 Hz (bottom left), and 20 Hz (bottom right) averaged from all animals (pooled data;  $n = 5$ ). To aid an intuitive understanding, the tertipin condition was designated as D(-) in this panel because tertipin blocked the direct action of ACh. S(+) indicates the presence of CSS. Significant interaction ( $P = 0.051$ ) were obtained at 5 and 10 Hz vagal stimulation, respectively, but not at 15 and 20 Hz vagal stimulation.

be insignificant in terms of physiological HR control.

#### Effect of CSS on the gain of vagal HR control via $K_{ACh}$ channels

Because the direct action of ACh via  $K_{ACh}$  is considered to be independent of sympathetic control [12], an accentuated antagonism is unlikely to occur in the direct action. However, because the interbeat interval is determined by the pacemaker potential of the sinus node cells, which in turn depends on all of the potassium, sodium, and calcium currents, there could be interaction between the  $K_{ACh}$  channel pathway and background sympathetic tone when we observe the HR response. Changes in the sodium current and/or calcium current induced by background sympathetic tone would modify the effect of changes in the potassium current through the  $K_{ACh}$  channels.

Our results indicate that accentuated antagonism occurred, affecting the direct action of ACh in the range of mild vagal stimulation as follows. In the dynamic protocol that was carried out with a mean vagal stimulation frequency of 5 Hz, significant positive interaction was observed between the tertipin and CSS effects, affecting the dynamic gain as well as the calculated maximum step

response (Table 2), suggesting that the effect of the  $K_{ACh}$  channel pathway was enhanced during CSS. The static protocol also showed significant positive interaction at 5 Hz vagal stimulation (Fig. 3B). The augmentation of the bradycardic response to vagal stimulation gained by the direct action of ACh through the  $K_{ACh}$  channels was enhanced under concomitant CSS.

The reason for the absence of a positive interaction between the tertipin and CSS effects at 15 and 20 Hz vagal stimulation is unclear (Fig. 3B). One possible explanation is the curvilinearity of the HR response to vagal stimulation. In the right panel of Fig. 3A, the tertipin-free control data (open symbols), which correspond to S(+)/D(+) in Fig. 3B, showed the steepest slope at the 0–5 Hz vagal stimulation step. The slope became shallower as the vagal stimulation frequency increased, suggesting a saturation phenomenon of HR reduction in response to vagal stimulation. It is very likely that such curvilinearity masked possible positive interaction between CSS and the direct action of ACh in determining the HR reduction during 15 and 20 Hz vagal stimulation. Accentuated antagonism in the direct action of ACh through  $K_{ACh}$  channels might therefore operate under balanced conditions of sympha-

thetic and vagal nerve activities.

The existence of an accentuated antagonism in the direct action of ACh through the  $K_{ACh}$  channels could be explained by macromolecular signaling complexes in which G protein-gated inwardly rectifying potassium (GIRK) channels are physically associated with signaling partner regulated by different G protein-coupled receptors (GPCRs) [19, 20]. Cardiac sympathetic stimulation simultaneously activates several different GPCRs:  $\alpha$ -adrenergic,  $\beta$ 1-adrenergic, and  $\beta$ 2-adrenergic receptors. Notably, the  $\beta$ 1-adrenergic receptor is coupled to downstream kinase, protein kinase A (PKA). The  $\beta$ -adrenergic signaling via PKA phosphorylation increases the activity of  $K_{ACh}$  channels [21, 22]. Taken together,  $\beta$ -adrenergic receptors might augment the activity of  $K_{ACh}$  channels via a PKA-dependent mechanism.

### Limitations

This study has several limitations. First, the data was obtained from anesthetized animals. Since anesthesia would affect the autonomic tone, the results may not be directly applicable to conscious animals. However, because we cut and stimulated the right cardiac sympathetic and vagal nerves, changes in autonomic outflow associated with anesthesia might not have significantly affected the present results.

Second, we blocked the  $K_{ACh}$  channels to examine the effect of background sympathetic tone on the direct effect of ACh through the  $K_{ACh}$  channels. On the other hand, if we had blocked the indirect effect of ACh through the cyclic AMP pathway, leaving the direct effect of ACh intact, and then examined the effect of background sympathetic tone on the HR response to vagal stimulation, the results might have been excessively straightforward. However, we could find no blocker for the indirect effect of ACh alone that was suitable for *in vivo* study at present. Further studies are required to directly examine the effect of background sympathetic tone on the direct effect of ACh through the  $K_{ACh}$  channels.

In conclusion, concomitant CSS affected no parameters of rapidity (i.e., the corner frequency in the frequency domain and the time constant in the time domain) of vagal HR control via  $K_{ACh}$  channels. Moreover, HR reduction in response to vagal stimulation via  $K_{ACh}$  channels was augmented by concomitant sympathetic stimulation at 5 Hz vagal stimulation. These findings suggest that the rapidity of response of the vagal HR control via  $K_{ACh}$  channels is invariant with respect to background sympathetic tone, and that the magnitude of vagal HR control via  $K_{ACh}$  channels is affected by background sympathetic tone *in vivo*.

This study was supported by Health and Labour Sciences Research Grants H15-Physi-001, H18-Nano-Ippan-003, and H18-Iryo-Ippan-023 from the Ministry of Health, Grants-in-Aid for Scientific Research promoted by the Ministry of Education, Culture, Sports, Science and Technology in Japan 18591992, 19700559, and by the Ground-based

Research Announcement for Space Utilization project promoted by the Japan Space Forum. This study was also supported by an Industrial Technology Research Grant Program in 06B44524a from the New Energy and Industrial Technology Development Organization of Japan.

### REFERENCES

- Luetjens CW, Tietje KM, Christian JL, Nathanson NM. Differential tissue expression and developmental regulation of guanine nucleotide binding regulatory proteins and their messenger RNAs in rat heart. *J Biol Chem.* 1988;263:13357-65.
- Sunahara RK, Dessauer CW, Gilman AG. Complexity and diversity of the mammalian adenylyl cyclases. *Annu Rev Pharmacol Toxicol.* 1996;36:461-80.
- Huang CL, Slesinger PA, Casey PJ, Jan YN, Jan LY. Evidence that direct binding of G beta gamma to the GIRK1 G protein-gated inwardly rectifying K<sup>+</sup> channel is important for channel activation. *Neuron.* 1995;15:1133-43.
- Sakmann B, Noma A, Trautwein W. Acetylcholine activation of single muscarinic K<sup>+</sup> channels in isolated pacemaker cells of the mammalian heart. *Nature.* 1983;303:250-3.
- Yamada M, Inanobe A, Kurachi Y. G protein regulation of potassium ion channels. *Pharmacol Rev.* 1998;50:723-60.
- Mizuno M, Kamiya A, Kawada T, Miyamoto T, Shimizu S, Sugimachi M. Muscarinic potassium channels augment dynamic and static heart rate responses to vagal stimulation. *Am J Physiol Heart Circ Physiol.* 2007;293:H1564-70.
- Negrão CE, Rondon MU, Tinucci T, Alves MJ, Roveda F, Braga AM, Reis SF, Nastari L, Barretto AC, Krieger EM, Middlekauff HR. Abnormal neurovascular control during exercise is linked to heart failure severity. *Am J Physiol Heart Circ Physiol.* 2001;280:H1286-92.
- Mancia G, Grassi G, Giannattasio C, Seravalle G. Sympathetic activation in the pathogenesis of hypertension and progression of organ damage. *Hypertension.* 1999;34:724-8.
- Seals DR, Bell C. Chronic sympathetic activation: consequence and cause of age-associated obesity? *Diabetes.* 2004;53:276-84.
- Hartzell HC, Méry PF, Fischmeister R, Szabo G. Sympathetic regulation of cardiac calcium current is due exclusively to cAMP-dependent phosphorylation. *Nature.* 1991;351:573-6.
- Irisawa H, Brown HF, Giles W. Cardiac pacemaking in the sinoatrial node. *Physiol Rev.* 1993;73:197-227.
- Breitwieser GE, Szabo G. Uncoupling of cardiac muscarinic and beta-adrenergic receptors from ion channels by a guanine nucleotide analogue. *Nature.* 1985;317:538-40.
- Levy MN. Sympathetic-parasympathetic interactions in the heart. *Circ Res.* 1971;29:437-45.
- Kawada T, Ikeda Y, Sugimachi M, Shishido T, Kawaguchi O, Yamazaki T, Alexander J Jr, Sunagawa K. Bidirectional augmentation of heart rate regulation by autonomic nervous system in rabbits. *Am J Physiol.* 1996;271:H288-95.
- Kawada T, Uemura K, Kashihara K, Jin Y, Li M, Zheng C, Sugimachi M, Sunagawa K. Uniformity in dynamic baroreflex regulation of left and right cardiac sympathetic nerve activities. *Am J Physiol Regul Integr Comp Physiol.* 2003;284:R1506-12.
- Brigham E. FFT transform applications. In: *The Fast Fourier Transform and its applications.* Englewood Cliffs, NJ: Prentice Hall; 1988. p. 167-203.
- Bendat J, Piersol A. Single-input/output relationships. In: *Random data: analysis and measurement procedures (3rd edition).* New York: Wiley; 2000. p. 189-217.
- Marmarelis V, Marmarelis V. The white noise method in system identification. In: *Analysis of physiological systems.* New York: Plenum; 1978. p. 131-221.
- Lavigne N, Ethier N, Oak JN, Pei L, Liu F, Trieu P, Rebois RV, Bouvier M, Hebert TE, Van Tol HH. G protein-coupled receptors form stable complexes with inwardly rectifying potassium channels and adenylyl cyclase. *J Biol Chem.* 2002;277:46010-9.
- Nikolov EN, Ivanova-Nikolova TT. Coordination of membrane excitability through a GIRK1 signaling complex in the atria. *J Biol Chem.* 2004;279:23630-6.
- Kim D. Beta-adrenergic regulation of the muscarinic-gated K<sup>+</sup> channel via cyclic AMP-dependent protein kinase in atrial cells. *Circ Res.* 1990;67:1292-8.
- Müllerner C, Vorobiov D, Bera AK, Uezono Y, Yakubovich D, Frohwiessner-Steinecker B, Dascal N, Schreibmayer W. Heterologous facilitation of G protein-activated K<sup>+</sup> channels by beta-adrenergic stimulation via cAMP-dependent protein kinase. *J Gen Physiol.* 2000;115:547-58.

## Contrasting effects of presynaptic $\alpha_2$ -adrenergic autoinhibition and pharmacologic augmentation of presynaptic inhibition on sympathetic heart rate control

Tadayoshi Miyamoto,<sup>1,2</sup> Toru Kawada,<sup>2</sup> Yusuke Yanagiya,<sup>2</sup> Tsuyoshi Akiyama,<sup>3</sup> Atsunori Kamiya,<sup>2</sup> Masaki Mizuno,<sup>2</sup> Hiroshi Takaki,<sup>2</sup> Kenji Sunagawa,<sup>4</sup> and Masaru Sugimachi<sup>2</sup>

<sup>1</sup>Department of Physical Therapy, Faculty of Health Sciences, Morinomiya University of Medical Sciences; and <sup>2</sup>Department of Cardiovascular Dynamics, Advanced Medical Engineering Center, and <sup>3</sup>Department of Cardiac Physiology, National Cardiovascular Center Research Institute, Osaka; and <sup>4</sup>Department of Cardiovascular Medicine, Graduate School of Medical Sciences, Kyusyu University, Fukuoka, Japan

Submitted 16 May 2008; accepted in final form 19 August 2008

Miyamoto T, Kawada T, Yanagiya Y, Akiyama T, Kamiya A, Mizuno M, Takaki H, Sunagawa K, Sugimachi M. Contrasting effects of presynaptic  $\alpha_2$ -adrenergic autoinhibition and pharmacologic augmentation of presynaptic inhibition on sympathetic heart rate control. *Am J Physiol Heart Circ Physiol* 295: H1855–H1866, 2008. First published August 29, 2008; doi:10.1152/ajpheart.522.2008.—Presynaptic  $\alpha_2$ -adrenergic receptors are known to exert feedback inhibition on norepinephrine release from the sympathetic nerve terminals. To elucidate the dynamic characteristics of the inhibition, we stimulated the right cardiac sympathetic nerve according to a binary white noise signal while measuring heart rate (HR) in anesthetized rabbits ( $n = 6$ ). We estimated the transfer function from cardiac sympathetic nerve stimulation to HR and the corresponding step response of HR, with and without the blockade of presynaptic inhibition by yohimbine (1 mg/kg followed by 0.1 mg·kg<sup>-1</sup>·h<sup>-1</sup> iv). We also examined the effect of the  $\alpha_2$ -adrenergic receptor agonist clonidine (0.3 and 1.5 mg·kg<sup>-1</sup>·h<sup>-1</sup> iv) in different rabbits ( $n = 5$ ). Yohimbine increased the maximum step response (from 7.2 ± 0.8 to 12.2 ± 1.7 beats/min, means ± SE,  $P < 0.05$ ) without significantly affecting the initial slope (0.93 ± 0.23 vs. 0.94 ± 0.22 beats·min<sup>-1</sup>·s<sup>-1</sup>). Higher dose but not lower dose clonidine significantly decreased the maximum step response (from 6.3 ± 0.8 to 6.8 ± 1.0 and 2.8 ± 0.5 beats/min,  $P < 0.05$ ) and also reduced the initial slope (from 0.56 ± 0.07 to 0.51 ± 0.04 and 0.22 ± 0.06 beats·min<sup>-1</sup>·s<sup>-1</sup>,  $P < 0.05$ ). Our findings indicate that presynaptic  $\alpha_2$ -adrenergic autoinhibition limits the maximum response without significantly compromising the rapidity of effector response. In contrast, pharmacologic augmentation of the presynaptic inhibition not only attenuates the maximum response but also results in a sluggish effector response.

systems analysis; transfer function;  $\alpha$ -adrenergic blockade; rabbits

PRESYNAPTIC  $\alpha_2$ -ADRENERGIC receptors play an important role in regulating neurotransmitter release in the central and peripheral nervous systems. The concept that neurotransmitter release is modulated by presynaptic autoreceptors was proposed in the 1970s (19, 20, 25, 31–33, 37, 38). Langer (18) first demonstrated that an  $\alpha$ -adrenergic antagonist phentolamine, at a concentration below that required to produce its negative chronotropic effect, increases the magnitude of heart rate (HR) response to sympathetic nerve stimulation. Since then, a number of *in vivo* and *in vitro* studies have

been conducted to characterize the negative feedback regulation of norepinephrine (NE) release via the presynaptic  $\alpha_2$ -adrenergic receptors located on the sympathetic nerve terminals (1, 6, 9, 11, 17, 24, 26, 27a, 29, 30, 34, 35). However, the dynamic nature of the presynaptic  $\alpha_2$ -adrenergic inhibition in sympathetic HR control remains to be quantified. Because we focus on the effector response to sympathetic nerve stimulation, the term “presynaptic” may be interpreted as “prejunctional” throughout this paper to describe more specifically the NE kinetics at the neuroeffector junction.

We first schematize our hypothesis on the possible modes of operations of the presynaptic inhibition. With reference to Fig. 1, the solid and dotted lines indicate the HR responses with and without the presynaptic inhibition, respectively. Figure 1A represents a “limiter-like” operation of the presynaptic inhibition in which the steady-state response is attenuated, while the initial slope of the response is unchanged. Figure 1B represents an “attenuator-like” operation in which the steady-state response is attenuated, while the initial slope of the response is also reduced in proportion to the attenuation of the steady-state response. Since the rapid effector response is one of the important hallmarks of neural regulation compared with humoral regulation, determining which of the two operations likely occurs would contribute to the physiological understanding of the presynaptic inhibition. The words “limiter-like” and “attenuator-like” in this paper are used in the specific senses described above.

To answer which of the two operations likely occurs in the presynaptic inhibition, we examined the HR response to dynamic sympathetic nerve stimulation, with or without blocking the  $\alpha_2$ -adrenergic receptors in anesthetized rabbits. Because the HR response is mainly mediated by the postsynaptic  $\beta_1$ -adrenergic receptors, the administration of an  $\alpha_2$ -adrenergic receptor antagonist does not eliminate the HR response to sympathetic nerve stimulation. We also examined the effects of pharmacologic augmentation of the  $\alpha_2$ -adrenergic receptors on the HR response to dynamic sympathetic nerve stimulation. The results of the present study indicated that the presynaptic  $\alpha_2$ -adrenergic autoinhibition is a limiter-like operation. In contrast, the pharmacologic

Address for reprint requests and other correspondence: T. Miyamoto, Dept. of Physical Therapy, Faculty of Health Sciences, Morinomiya Univ. of Medical Sciences, Osaka 559-8611, Japan (e-mail: miyamoto@morinomiya-u.ac.jp).

The costs of publication of this article were defrayed in part by the payment of page charges. The article must therefore be hereby marked “advertisement” in accordance with 18 U.S.C. Section 1734 solely to indicate this fact.

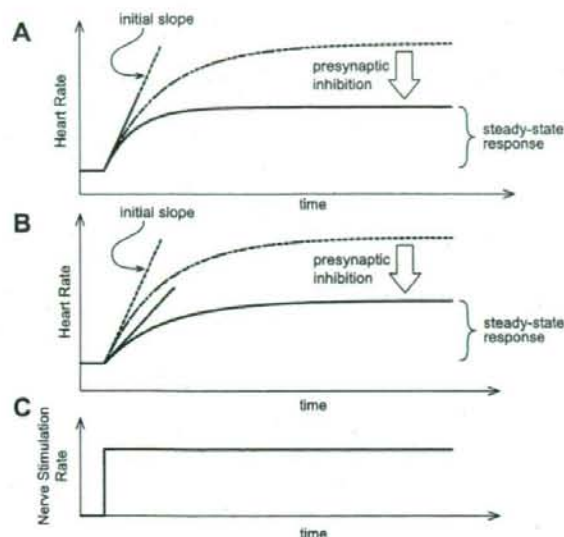


Fig. 1. Schematic representations of the possible operations of the presynaptic inhibition in heart rate (HR) step response to sympathetic nerve stimulation. The solid and dashed lines indicate the HR step response with and without the presynaptic inhibition, respectively. *A*: the presynaptic inhibition attenuates the steady-state response without affecting the initial slope of the response (a "limiter-like" operation). *B*: the presynaptic inhibition attenuates the steady-state response accompanied by a decrease in the initial slope in proportion to the attenuation of the steady-state response (an "attenuator-like" operation). Rapid effector response is maintained in the former but not in the latter. *C*: postulated nerve stimulation rate.

augmentation of presynaptic inhibition is an attenuator-like operation. A possible theoretical explanation for the difference in dynamic characteristics between the presynaptic  $\alpha_2$ -adrenergic autoinhibition and the pharmacologic augmentation of the presynaptic inhibition will be proposed.

## METHODS

### Surgical Preparations

Animal care was in accordance with "Guiding Principles for the Care and Use of Animals in the Field of Physiological Sciences," approved by the Physiological Society of Japan. All protocols were reviewed and approved by the Animal Subject Committee of the National Cardiovascular Center. Japanese white rabbits, weighing 2.5–3.1 kg, were anesthetized by intravenous injection (2 ml/kg) of a mixture of urethane (250 mg/ml) and  $\alpha$ -chloralose (40 mg/ml) and mechanically ventilated with oxygen-enriched room air. Tidal volume was set at 35 ml and the rate was adjusted between 35 and 40 cycles/min to be sufficient for suppressing spontaneous respiration. Supplemental doses of these anesthetics were administered by continuous intravenous infusion (1 ml·kg<sup>-1</sup>·h<sup>-1</sup>) into the marginal ear vein. Arterial pressure (AP) was monitored with a micromanometer catheter (model, Millar Instruments, Houston, TX) inserted into the right femoral artery. A catheter for drug administration was also placed in the right femoral vein. Sinoaortic denervation was performed bilaterally to minimize changes in systemic sympathetic activity via the arterial baroreflexes. The vagi were also sectioned bilaterally at the neck level to remove the vagal control on HR. The right inferior cardiac sympathetic nerve was exposed through a mid-line thoracotomy and sectioned. A pair of bipolar platinum electrodes was then attached to the cardiac end of the sectioned sympathetic

nerve for stimulation (12, 13, 22, 23). The stimulation electrodes and nerve were secured with silicon glue (Kwik-Sil, World Precision Instruments, Sarasota, FL). Instantaneous HR was measured from the AP signal utilizing a cardiachometer (Tachometer N4778, San-ei, Tokyo, Japan). Body temperature was maintained at 38°C with a heating pad throughout the experiment.

### Experimental Procedures

**Protocols.** To estimate the transfer function from the sympathetic nerve stimulation to HR response, we employed a binary white noise stimulation signal with a switching interval of 5 s. The power spectrum of the sympathetic nerve stimulation rate was fairly constant up to 0.1 Hz and decreased to  $\sim 1/10$  at 0.15 Hz. The upper frequency limit of the input power that covers the frequency range of physiological interest was determined based on our laboratory's previous studies (12, 23) and also preliminary experimental runs. Different sequences of binary white noise signals were used in different animals. Because HR is linearly related to cardiac output when stroke volume is unchanged, we chose HR as an output signal to understand sympathetic cardiovascular regulation. However, to rule out the possibility that the reciprocal relationship between R-R interval (RRI) and HR confounded the analytical results, we also calculated the transfer function using RRI as an output signal.

In *protocol 1* ( $n = 6$ ), to examine the dynamic nature of the presynaptic  $\alpha_2$ -adrenergic autoinhibition, we estimated the transfer function from dynamic sympathetic nerve stimulation to HR response from 20-min data obtained under control and  $\alpha_2$ -adrenergic blockade conditions as follows. After recording the control data, an  $\alpha_2$ -adrenergic antagonist yohimbine was administered intravenously with an initial bolus injection of 1 mg/kg, followed by continuous infusion at 0.1 mg·kg<sup>-1</sup>·h<sup>-1</sup>. The yohimbine bolus was equivalent to 10 h of infusion. The duration from the initiation of yohimbine administration until HR and AP reached new steady-state levels was  $\sim 15$  min (35). We then repeated the 20-min dynamic sympathetic nerve stimulation and recorded the HR response under the  $\alpha_2$ -adrenergic blockade condition.

In *protocol 2* ( $n = 5$ ), to examine the effects of pharmacologic augmentation of the presynaptic  $\alpha_2$ -adrenergic inhibition on the sympathetic HR control, we estimated the transfer function from dynamic sympathetic nerve stimulation to HR response before and during the administration of an  $\alpha_2$ -adrenergic receptor agonist clonidine. Clonidine was administered intravenously at 0.3 and 1.5 mg·kg<sup>-1</sup>·h<sup>-1</sup> in an increasing order. After 20-min baseline data collection, we started lower dose clonidine administration and waited for 15 min and then collected data for 20 min. Next, we started higher dose clonidine administration and waited for 15 min and then collected data for 20 min.

The stimulation rate of binary white noise was set at 0–1 Hz for *protocol 1*, and 0–5 Hz for *protocol 2*. Because we expected that blockade of the presynaptic  $\alpha_2$ -adrenergic inhibition would augment, whereas activation of the inhibition would attenuate, the HR response, we set a higher stimulation rate for *protocol 2* than for *protocol 1*. The pulse width of sympathetic stimulation was set at 2 ms. The amplitude was set so that 5-Hz tonic sympathetic stimulation produced a HR increase of  $\sim 50$  beats/min.

As a supplemental protocol, we performed the transfer function analysis using binary white noise signals of 0–1 Hz (Bin<sub>0.1</sub>), 0–3 Hz (Bin<sub>0.3</sub>), and 0–5 Hz (Bin<sub>0.5</sub>) in a random order ( $n = 5$ ). At least a 15-min interval was allowed between the 20-min dynamic sympathetic stimulation trials. The amplitude of sympathetic stimulation was set so that 1-Hz tonic sympathetic stimulation produced a HR increase of  $\sim 50$  beats/min.

Medetomidine has higher affinity to  $\alpha_2$ -adrenergic receptors over  $\alpha_1$ -adrenergic receptors compared with clonidine ( $\alpha_2/\alpha_1 = 1,620:1$  for medetomidine, 220:1 for clonidine) (28). However, a preliminary experiment indicated that medetomidine was not as effective as



clonidine to modulate the transfer function from dynamic sympathetic stimulation to HR. Accordingly, we examined the effects of clonidine or medetomidine on myocardial interstitial NE release in response to 5-Hz tonic stimulation (2.5 V, 2-ms pulse width) of the right cardiac sympathetic nerve in vagotomized rabbits. Two microdialysis probes were implanted in the myocardium of the left ventricular free wall. Ringer solution was perfused at 2  $\mu\text{l}/\text{min}$ . After a 2-h equilibrium period, we collected 5-min dialysate samples to measure the dialysate NE concentration as an index of myocardial interstitial NE levels (14, 15). High-performance liquid chromatography with electrochemical detection was used to quantify the NE concentration. After the sympathetic stimulation was performed under the control condition, clonidine or medetomidine was intravenously administered (1.5  $\text{mg}\cdot\text{kg}^{-1}\cdot\text{h}^{-1}$ ). Fifteen minutes later, the sympathetic stimulation was performed under the drug administration condition. Then the drug administration was ceased. Forty-five minutes later, the sympathetic stimulation was performed under the recovery condition. We used different rabbits for clonidine and medetomidine trials. We pooled six dialysate data for statistical analysis.

#### Data Analysis

Data were digitized at 200 Hz utilizing a 12-bit analog-to-digital converter and stored on the hard disk of a dedicated laboratory computer system. Mean values for HR and AP during dynamic sympathetic nerve stimulation were calculated by averaging the respective data over the stimulation period.

The transfer function from dynamic sympathetic nerve stimulation to HR response was estimated by the following procedures. Twenty minutes of input data (stimulation command) and output data (HR) were resampled at 8 Hz. The resampled data were segmented into eight 50% overlapping bins consisting of 2,048 data points each. The segment length was 256 s. For each segment, the linear trend was subtracted, and a Hanning window was applied. Fast-Fourier transform was then performed to obtain the frequency spectrum of nerve stimulation rate  $[N(f)]$  and that of HR  $[HR(f)]$  (5). The power spectral density of the nerve stimulation rate  $[S_{N-N}(f)]$ , that of HR  $[S_{HR-HR}(f)]$ , as well as the cross-spectral density between these two signals  $[S_{N-HR}(f)]$ , were averaged over the eight segments. Finally, the transfer function  $[H(f)]$  from sympathetic nerve stimulation rate to HR response was calculated using the following equation (2, 21).

$$H(f) = \frac{S_{N-HR}(f)}{S_{N-N}(f)} \quad (1)$$

Transfer function parameters were determined by fitting a second-order, low-pass filter to the estimated transfer function, according to previous studies (12, 13, 23). The second-order, low-pass filter with a pure dead time  $[G(f)]$  is expressed as

$$G(f) = \frac{K}{1 + 2\zeta \frac{f}{f_N} + \left(\frac{f}{f_N}\right)^2} \exp(-2\pi f j L) \quad (2)$$

where  $K$  is a steady-state gain,  $f_N$  is natural frequency (in Hz),  $\zeta$  is a damping ratio,  $L$  is pure dead time (in s), and  $j$  indicates an imaginary unit. A schematic explanation for these transfer function parameters is provided in the APPENDIX. To estimate the parameters, an iterative nonlinear least squares fitting was performed to minimize the following error function.

$$\text{error} = \frac{\sum_{k=1}^n |G(f) - H(f)|^2}{\sum_{k=1}^n |H(f)|^2}, \quad f = f_0 \times k \quad (3)$$

where  $f_0$  is the fundamental frequency of the discrete Fourier transform,  $f_0 = 1/256 = 0.004$  Hz, and  $k$  is a frequency index. The  $n$

represents the upper limit of the frequency index determined from the range of sufficient input power in the sympathetic nerve stimulation;  $n = 40$ ,  $f_0 \times n = 0.156$  Hz.

To quantify the linear dependence of the HR response on the sympathetic nerve stimulation, the magnitude-squared coherence function  $[\gamma^2(f)]$  was calculated by the following equation (2, 21).

$$\gamma^2(f) = \frac{|S_{N-HR}(f)|^2}{S_{N-N}(f) \cdot S_{HR-HR}(f)} \quad (4)$$

The coherence value ranges from zero to unity. The unity coherence value indicates a perfect linear dependence between the input and output signals, whereas zero coherence indicates a total independence between the two signals.

To facilitate the intuitive understanding of the HR response to dynamic sympathetic nerve stimulation, we calculated the step response from the estimated transfer function. The step response was obtained from the time integral of the system impulse response derived from the inverse Fourier transform of the transfer function. The steady-state response was calculated by averaging the step response during the last 10 s of the 128-s response. To characterize the rising speed of the step response, the initial slope for the response was calculated as follows. An analysis of linear regression with a slope and an intercept was performed on the initial data points of the step response while varying the number of data points from 2 to 1,024. The maximum slope obtained was used as the initial slope of the response. The linear regression was performed, including the portion of the dead time. Although including the dead time reduced the maximum slope, the effect was small because the number of data points that yielded the maximum slope ( $\sim 90$  points) was much larger than that for the dead time ( $< 10$  points). The step response of RRI was also calculated from the corresponding transfer function from sympathetic nerve stimulation to RRI.

#### Statistics

All data are presented as means  $\pm$  SE. In *protocol 1*, mean HR, AP, and transfer function parameters were compared before and during yohimbine administration by paired *t*-tests. In *protocol 2*, the data were compared among control, lower dose, and higher dose clonidine conditions using a repeated-measures ANOVA followed by Dunnett's test against the single control (8). In the supplemental protocol of the transfer function analysis, the data were compared among  $\text{Bin}_{0.1}$ ,  $\text{Bin}_{0.3}$ , and  $\text{Bin}_{0.5}$  stimulus conditions using a repeated-measures ANOVA followed by Tukey test for all pairwise comparisons. In the supplemental protocol of the NE measurement, baseline NE levels were compared before and during drug administration using a paired *t*-test. The NE levels during sympathetic stimulation were compared among control, drug administration, and recovery conditions using a repeated-measures ANOVA followed by Dunnett's test against the control condition. In all of the statistical procedures, the difference was considered significant at  $P < 0.05$ .

#### RESULTS

Figure 2A represents a typical recording obtained from *protocol 1*. We stimulated the cardiac sympathetic nerve according to a binary white noise signal and recorded HR response under control condition and during yohimbine administration. The presynaptic  $\alpha_2$ -adrenergic negative feedback mechanism functioned under the control condition but not during yohimbine administration. HR changed dynamically in response to the random sympathetic nerve stimulation under both conditions. Yohimbine increased the magnitude of HR variation. The augmentation of sympathetic effect was also observed in the RRI response. Although yohimbine decreased the mean level of HR in this animal, changes in mean HR

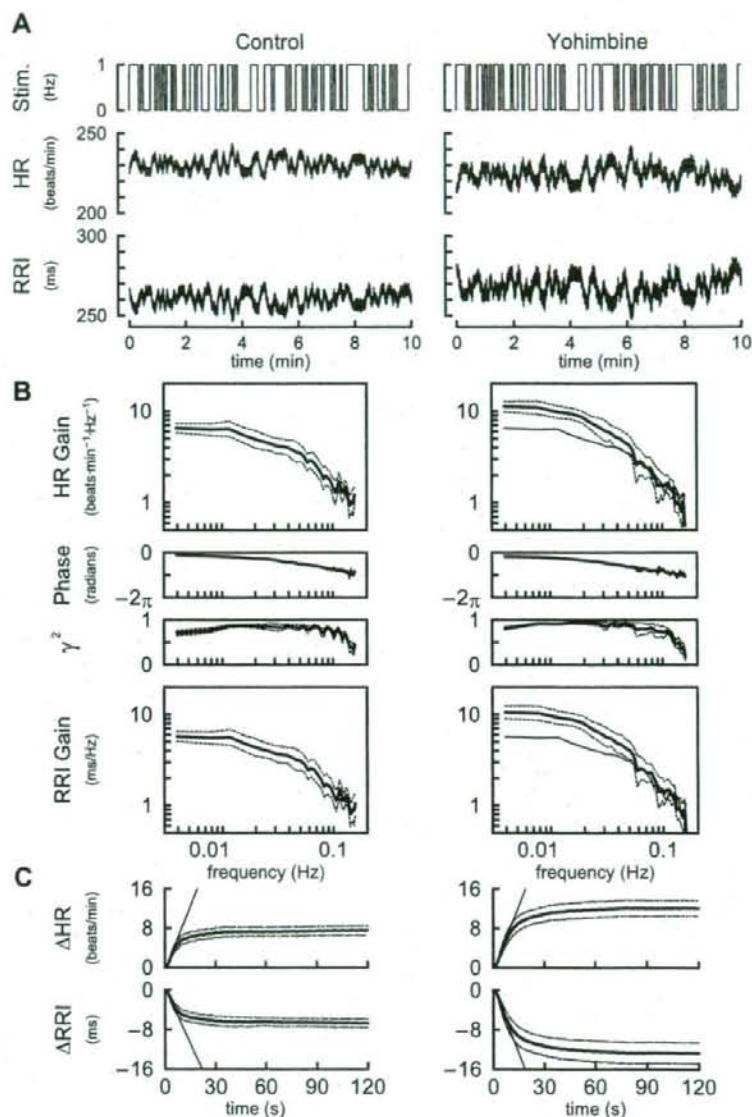


Fig. 2. *A:* representative recordings of cardiac sympathetic nerve stimulation rate (Stim; *top*), HR response (*middle*), and R-R interval (RRI) response (*bottom*) under conditions of control (*left*) and yohimbine administration (*right*) obtained in *protocol 1*. Yohimbine blocks the presynaptic  $\alpha_2$ -adrenergic autoinhibition. The amplitude of HR variation and that of RRI variation become greater in the presence of yohimbine. *B:* transfer functions averaged over all animals in *protocol 1*. HR gain plots (*top*), phase plots (*second*), coherence functions ( $\gamma^2$ , *third*), and RRI gain plots (*bottom*). Yohimbine increases the dynamic gain in the frequency range between 0.004 and 0.04 Hz but not in the higher frequency range. The fine solid curve in the gain (*right*) duplicates the mean gain plot (*left*). *C:* step responses of HR (*top*) and RRI (*bottom*) calculated from the corresponding transfer functions. Yohimbine augments the steady-state response without affecting the initial slope of the response (fine oblique line). Bold, solid lines represent the mean, whereas dotted lines indicate means  $\pm$  SE.

varied among the animals and were not significantly different between the control and yohimbine conditions.

Table 1 summarizes the mean HR and AP averaged from the six animals. The  $\alpha_2$ -adrenergic blockade by yohimbine did not significantly affect the HR or AP before sympathetic nerve stimulation. Yohimbine also did not affect HR or AP significantly during the stimulation period.

Figure 2*B* illustrates the transfer functions averaged from the six animals in *protocol 1*. In the HR gain plots, the gain value was relatively constant  $<0.01$  Hz and decreased  $>0.01$  Hz, indicating low-pass filter characteristics of the HR response to sympathetic nerve stimulation. Yohimbine increased the HR gain from  $7.1 \pm 0.7$  to  $12.0 \pm 1.7$  beats  $\cdot$  min $^{-1}$   $\cdot$  Hz $^{-1}$  at the

lowest frequency of 0.004 Hz ( $P < 0.05$ ). In contrast, yohimbine did not affect the HR gain value at 0.1 Hz ( $1.8 \pm 0.4$  vs.  $1.7 \pm 0.6$  beats  $\cdot$  min $^{-1}$   $\cdot$  Hz $^{-1}$ ). The solid fine curve in the *right* panel duplicates the mean gain plot in the *left* panel as a reference. In the phase plots, the phase value approached zero radians at the lowest frequency and lagged with increasing frequency under both conditions. In the coherence function plots, the coherence was  $>0.8$  in the frequency range from 0.01 to 0.08 Hz, suggesting that the HR response to sympathetic nerve stimulation in this frequency range can be explained reasonably well by linear dynamics for both conditions. Changes in the RRI gain plots were similar to those in the HR gain plots. Yohimbine increased the RRI gain from

Table 1. Mean heart rate and arterial pressure before and during random stimulation of the cardiac sympathetic nerve

	Control	Yohimbine
Heart rate, beats/min		
Before	259 ± 15	244 ± 13
During	264 ± 15	254 ± 17
Mean arterial pressure, mmHg		
Before	90 ± 8	87 ± 6
During	91 ± 9	88 ± 8

Values are means ± SE. Data were obtained after vagal and cardiac sympathetic nerves were cut. No statistically significant difference was detected between control vs. yohimbine values by paired *t*-tests.

6.0 ± 0.7 to 11.3 ± 1.9 ms/Hz at the lowest frequency of 0.004 ( $P < 0.05$ ) but not at 0.1 Hz (1.8 ± 0.4 vs. 1.9 ± 0.8 ms/Hz). Given the inverse relationship between RRI and HR, the RRI phase plots (not shown) quite resembled to the corresponding HR phase plots except for the rotation by  $\pi$  radians.

Figure 2C represents the step responses of HR to sympathetic nerve stimulation calculated from the transfer functions shown in Fig. 2B. Yohimbine increased the steady-state response significantly (Table 2). The initial slope of the response, depicted by an oblique straight line, was not affected by yohimbine (Table 2). In the RRI step response, yohimbine augmented the steady-state response from  $-6.7 \pm 0.9$  to  $-12.6 \pm 2.1$  ms ( $P < 0.05$ ) without affecting the initial slope ( $-0.71 \pm 0.18$  vs.  $-0.90 \pm 0.23$  ms/s).

Parameters of the transfer functions and step responses estimated in protocol 1 are summarized in Table 2. The steady-state gain was significantly greater and the natural frequency was significantly lower in yohimbine condition compared with control. The damping coefficient and pure dead time did not differ significantly between the control and yohimbine conditions. Whereas the steady-state response was significantly increased by yohimbine, the initial slope of the step response was not significantly changed.

Figure 3A represents a typical recording of the sympathetic nerve stimulation and HR response obtained from protocol 2. The effects of  $\alpha_2$ -adrenergic stimulation by clonidine were tested at two doses. Lower dose clonidine did not affect the magnitude of HR variation. Although lower dose clonidine decreased the mean HR in this animal, changes in the mean HR were not significantly different among the animals (Table 3). Higher dose clonidine significantly attenuated the magnitude of HR variation and also decreased mean HR. The attenuation of sympathetic effect was also observed in the RRI response during the high-dose clonidine administration.

Table 3 summarizes the mean HR and AP obtained from protocol 2. Higher dose, but not lower dose, clonidine significantly decreased the mean HR, both before and during cardiac sympathetic nerve stimulation. Clonidine did not affect mean AP significantly, before or during cardiac sympathetic nerve stimulation.

Figure 3B illustrates the transfer functions averaged from the five animals in protocol 2. Lower dose clonidine did not affect the transfer function significantly. In the HR gain plots, higher dose clonidine decreased the gain from  $6.6 \pm 0.9$  to  $2.7 \pm 0.5$  beats·min<sup>-1</sup>·Hz<sup>-1</sup> at the lowest frequency of 0.004 Hz ( $P < 0.05$ ) and from  $1.1 \pm 0.2$  to  $0.5 \pm 0.2$  beats·min<sup>-1</sup>·Hz<sup>-1</sup> at the frequency of 0.1 Hz ( $P < 0.05$ ). Higher dose clonidine did not

affect the phase plot significantly. In the coherence function plots, the coherence was  $>0.8$  in control and lower dose clonidine conditions and  $>0.7$  in higher dose clonidine condition for the frequency range from 0.01 to 0.08 Hz, suggesting that the HR response to sympathetic nerve stimulation can be explained reasonably well by linear dynamics in all three conditions. Although relative change became smaller compared to the HR gain plots, the attenuation of transfer gain was also observed in the RRI gain plots. Higher-dose clonidine decreased the gain from  $4.5 \pm 0.7$  to  $2.8 \pm 0.5$  ms/Hz at the lowest frequency of 0.004 Hz ( $P < 0.05$ ) and from  $0.88 \pm 0.19$  to  $0.04 \pm 0.09$  ms/Hz at the frequency of 0.1 Hz ( $P < 0.05$ ).

Figure 3C represents the step responses of HR to sympathetic nerve stimulation calculated from the transfer functions shown in Fig. 3B. Lower dose clonidine did not affect either the steady-state response or the initial slope of the step response. In contrast, higher dose clonidine attenuated the steady-state response and also reduced the initial slope of the response. In the RRI step response, higher-dose clonidine attenuated the steady-state response from  $-4.9 \pm 0.7$  to  $-3.0 \pm 0.6$  ms ( $P < 0.05$ ) with a significant reduction in the initial slope from  $-0.40 \pm 0.07$  to  $-0.23 \pm 0.05$  ms/s ( $P < 0.05$ ).

Parameters of the transfer functions and step responses estimated in protocol 2 are summarized in Table 4. The steady-state gain of the transfer function and the steady-state response of the corresponding step response were decreased by higher dose but not by lower dose clonidine. The initial slope of the step response was decreased by higher dose clonidine. The ratio of the steady-state response to the initial slope was unchanged. The natural frequency and the damping ratio of the transfer function were not affected by clonidine. The pure dead time of the transfer function was increased by lower dose, but not by higher dose, clonidine.

Figure 4A represents a typical recording of the sympathetic nerve stimulation and HR response obtained from the supplemental protocol. The binary white noise signals of the same sequence but different stimulus rate were applied. Increasing the stimulus rate augmented the magnitude of HR variation and increased mean HR. The increase was not proportional to the increase in the stimulus rate, however, because of the saturation of HR response to sympathetic nerve stimulation. The increase of RRI variation was not proportional to the increase in the stimulus rate either, suggesting that the saturation effect observed in the HR response was not an artifact of reciprocal relationship between RRI and HR.

Table 2. Parameters of the transfer functions and step responses

	Control	Yohimbine
<i>K</i> , beats·min <sup>-1</sup> ·Hz <sup>-1</sup>	7.3 ± 1.1	12.0 ± 2.1*
<i>f<sub>n</sub></i> , Hz	0.081 ± 0.012	0.055 ± 0.008*
$\zeta$	1.64 ± 0.47	1.55 ± 0.21
<i>L</i> , s	0.82 ± 0.22	1.03 ± 0.19
Fitting error, %	5.6 ± 1.5	3.6 ± 1.1
<i>S</i> , beats/min	7.2 ± 0.8	12.2 ± 1.7*
$\alpha$ , beats·min <sup>-1</sup> ·s <sup>-1</sup>	0.93 ± 0.23	0.94 ± 0.22
<i>S</i> / $\alpha$ , s	9.1 ± 1.4	14.4 ± 1.9*

Values are means ± SE. *K*, steady-state gain; *f<sub>n</sub>*, natural frequency;  $\zeta$ , damping coefficient; *L*, pure dead time; *S*, steady-state response;  $\alpha$ , initial slope; *S*/ $\alpha$ , ratio of *S* to  $\alpha$ . \* $P < 0.05$  vs. control values.

Fig. 3. A: representative recordings of cardiac sympathetic nerve stimulation rate (top), HR response (middle), and RRI response (bottom) under conditions of control (left), lower-dose clonidine ( $0.3 \text{ mg}\cdot\text{kg}^{-1}\cdot\text{h}^{-1}$ ; middle), and higher-dose clonidine ( $1.5 \text{ mg}\cdot\text{kg}^{-1}\cdot\text{h}^{-1}$ ; right) obtained in protocol 2. Clonidine activates the presynaptic  $\alpha_2$ -adrenergic inhibition independent of the amount of norepinephrine released at the sympathetic nerve terminals. The amplitude of HR variation becomes smaller, and the mean level of HR becomes lower in the presence of higher-dose clonidine. The amplitude of RRI response also became smaller under higher-dose clonidine condition. B: transfer functions averaged over all animals in protocol 2. HR gain plots (top), phase plots (second), coherence functions ( $\gamma_2$ , third), and RRI gain plots (bottom). Lower-dose clonidine does not affect the transfer function significantly. Higher-dose clonidine decreases the dynamic gain in the whole frequency range (0.004 to 0.2 Hz). The fine solid curves in the gain plots (middle and right) duplicate the mean gain plot (left). C: step responses of HR (top) and RRI (bottom) calculated from the corresponding transfer functions. Lower-dose clonidine does not affect the step response significantly. Higher-dose clonidine attenuates the steady-state response accompanied by a decrease in the initial slope of the response (fine oblique line). Bold, solid lines represent the mean, whereas dotted lines indicate means  $\pm$  SE.

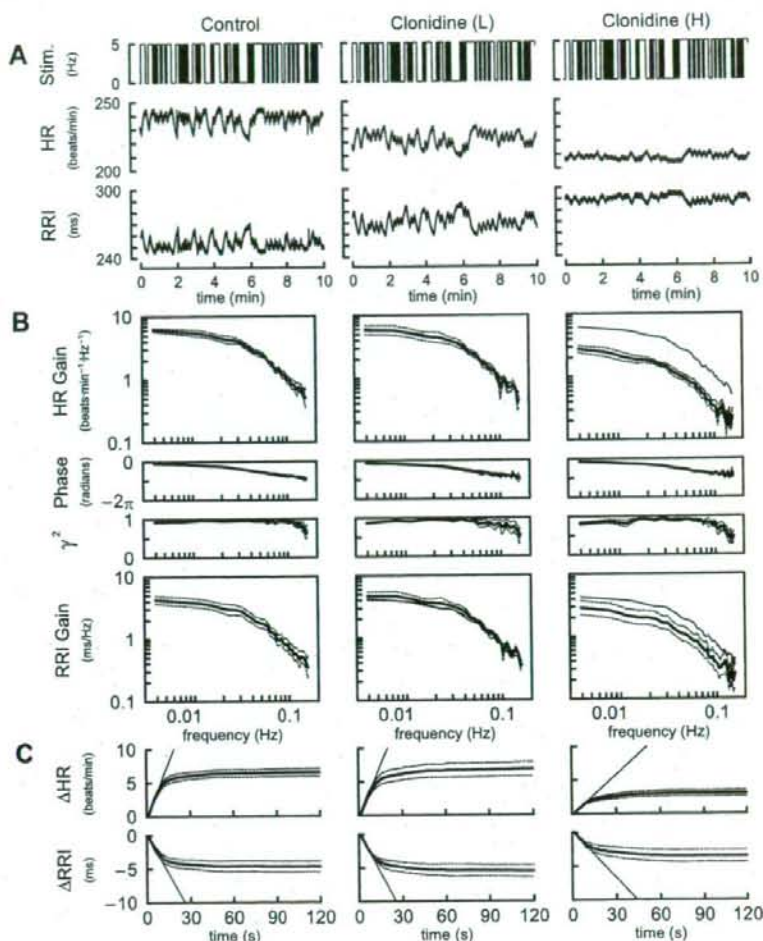


Table 5 summarizes the mean HR and AP obtained from the supplemental protocol. There were no significant differences in mean HR and AP before cardiac sympathetic nerve stimulation. Mean HR was higher in Bin<sub>0.3</sub> and Bin<sub>0.5</sub> than in Bin<sub>0.1</sub> condition. Mean AP did not differ among the three conditions.

Figure 4B illustrates the transfer function averaged from the five animals in the supplemental protocol. The contour of HR gain plots showed an approximately downward shift with

increase in the stimulus rate of the binary white noise signal, indicating that the augmentation of the HR variation seen in Fig. 4A was not proportional to the increase in the stimulus rate. No significant differences were noted in the phase plot. The coherence values were slightly decreased in all frequencies with increase in the stimulus rate of the binary white noise signal, suggesting that the HR response became saturated and the linearity between the stimulation and the HR response was

Table 3. Mean heart rate and arterial pressure before and during random stimulation of the cardiac sympathetic nerve

	Control	Clonidine (L)	Clonidine (H)
Heart rate, beats/min			
Before	277 ± 16	250 ± 15	232 ± 20*
During	299 ± 14	271 ± 14	246 ± 27*
Mean arterial pressure, mmHg			
Before	95 ± 6	77 ± 8	113 ± 9
During	96 ± 6	79 ± 9	115 ± 13

Values are means  $\pm$  SE. Data were obtained after vagal and cardiac sympathetic nerves were cut. \* $P < 0.05$  vs. control values by Dunnett's test.

Table 4. Transfer function parameters and step responses

	Control	Clonidine (L)	Clonidine (H)
$K$ , beats $\cdot$ min <sup>-1</sup> $\cdot$ Hz <sup>-1</sup>	6.4 ± 0.8	6.8 ± 1.1	2.7 ± 0.5*
$f_N$ , Hz	0.066 ± 0.017	0.070 ± 0.016	0.059 ± 0.013
$\zeta$	1.56 ± 0.37	1.72 ± 0.23	1.55 ± 0.20
$L$ , s	0.56 ± 0.17	1.24 ± 0.20*	1.03 ± 0.18
Fitting error, %	2.9 ± 1.2	4.2 ± 1.5	5.5 ± 2.3
$S$ , beats/min	6.3 ± 0.8	6.8 ± 1.0	2.8 ± 0.5*
$\alpha$ , beats $\cdot$ min <sup>-1</sup> $\cdot$ s <sup>-1</sup>	0.56 ± 0.07	0.51 ± 0.04	0.22 ± 0.06*
$S/\alpha$ , s	11.2 ± 0.7	13.1 ± 1.3	13.8 ± 1.2

Values are means  $\pm$  SE. \* $P < 0.05$  vs. control values.

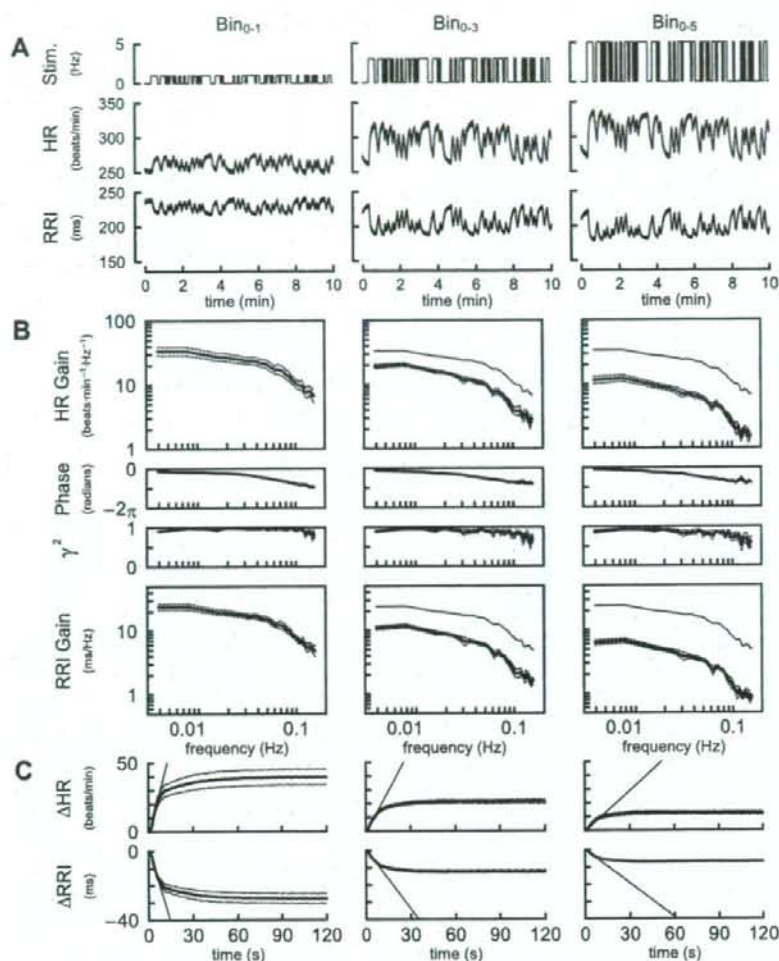


Fig. 4. *A*: representative recordings of cardiac sympathetic nerve stimulation rate (*top*), HR response (*middle*), and RRI response (*bottom*) obtained by differencing the stimulus rate of the binary white noise signal. *Bin*<sub>0.1</sub>, binary white noise between 0 and 1 Hz; *Bin*<sub>0.3</sub>, binary white noise between 0 and 3 Hz; *Bin*<sub>0.5</sub>, binary white noise between 0 and 5 Hz. Increasing the stimulus rate of the binary white noise signal augments the magnitude of HR response and increased mean HR. The RRI response was also increased with increasing the stimulus rate. *B*: transfer functions averaged over all animals in the supplemental protocol. HR gain plots (*top*), phase plots (*second*), coherence functions ( $\gamma^2$ , *third*), and RRI gain plots (*bottom*). Increasing the stimulus rate of the binary white noise signal decreases the dynamic gain in the whole frequency range (0.004 to 0.2 Hz). The fine solid curves in the gain plots (*middle and right*) duplicate the mean gain plot (*left*). *C*: step responses of HR (*top*) and RRI (*bottom*) calculated from the transfer functions. Increasing the stimulus rate of the binary white noise signal attenuates the steady-state response accompanied by a decrease in the initial slope of the response (fine oblique line). Bold, solid lines represent the mean, whereas dotted lines indicate means  $\pm$  SE.

slightly reduced in *Bin*<sub>0.3</sub> and *Bin*<sub>0.5</sub> compared with that in *Bin*<sub>0.1</sub> condition. The contour of RRI gain plots also showed approximately downward shift with increasing the stimulus rate of the binary white noise signal.

Table 5. Mean heart rate and arterial pressure before and during random stimulation of the cardiac sympathetic nerve

	<i>Bin</i> <sub>0.1</sub>	<i>Bin</i> <sub>0.3</sub>	<i>Bin</i> <sub>0.5</sub>
Heart rate, beats/min			
Before	268 $\pm$ 6	269 $\pm$ 7	266 $\pm$ 5
During	292 $\pm$ 8	330 $\pm$ 9*	341 $\pm$ 11*
Mean arterial pressure, mmHg			
Before	84 $\pm$ 7	82 $\pm$ 5	88 $\pm$ 12
During	94 $\pm$ 7	94 $\pm$ 7	95 $\pm$ 9

Values are means  $\pm$  SE. Data were obtained after vagal and cardiac sympathetic nerves were cut. *Bin*<sub>0.1</sub>, *Bin*<sub>0.3</sub>, and *Bin*<sub>0.5</sub>: binary white noise signals of 0–1, 0–3, and 0–5 Hz, respectively. \**P* < 0.01 vs. *Bin*<sub>0.1</sub> values by Tukey test. There were no significant differences in parameters between *Bin*<sub>0.3</sub> and *Bin*<sub>0.5</sub>.

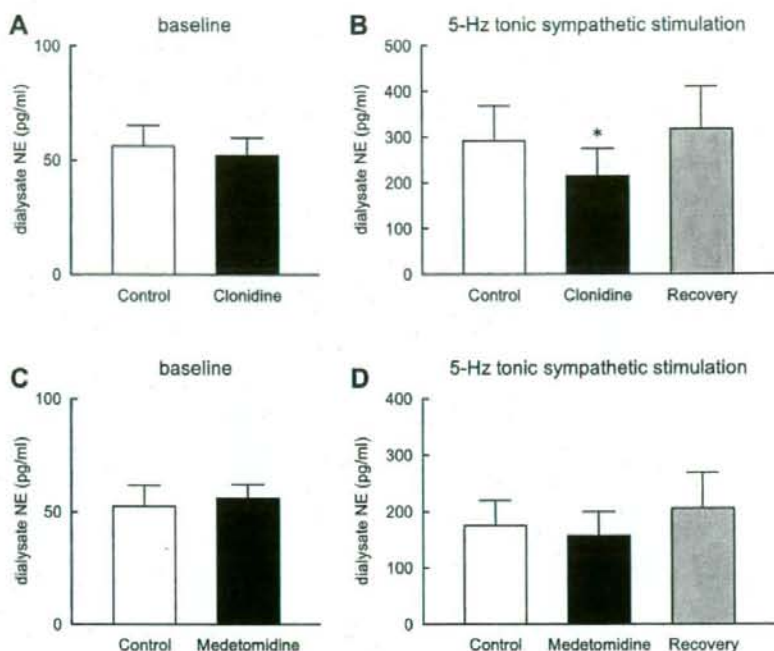
Figure 4C represents the step response of HR to sympathetic nerve stimulation calculated from the transfer functions shown in Fig. 4B. The increase in the stimulus rate of the binary white noise signal attenuated the steady-state response and also reduced the initial slope of the response. In the RRI step

Table 6. Transfer function parameters and step responses

	<i>Bin</i> <sub>0.1</sub>	<i>Bin</i> <sub>0.3</sub>	<i>Bin</i> <sub>0.5</sub>
<i>K</i> , beats $\cdot$ min <sup>-1</sup> $\cdot$ Hz <sup>-1</sup>	36.2 $\pm$ 4.9	20.0 $\pm$ 1.1†	11.8 $\pm$ 1.1†
<i>f</i> <sub>50</sub> , Hz	0.098 $\pm$ 0.009	0.079 $\pm$ 0.006*	0.078 $\pm$ 0.006*
<i>Z</i>	1.56 $\pm$ 0.04	1.68 $\pm$ 0.04*	1.68 $\pm$ 0.05*
<i>L</i> , s	0.95 $\pm$ 0.01	0.97 $\pm$ 0.01	0.97 $\pm$ 0.01
Fitting error, %	4.8 $\pm$ 1.1	3.2 $\pm$ 0.8	3.5 $\pm$ 0.5
<i>S</i> , beats/min	40.9 $\pm$ 5.1	22.1 $\pm$ 1.6†	12.8 $\pm$ 1.4†
$\alpha$ , beats $\cdot$ min <sup>-1</sup> $\cdot$ s <sup>-1</sup>	4.23 $\pm$ 0.61	2.00 $\pm$ 0.21†	1.20 $\pm$ 0.17†
<i>S</i> / $\alpha$ , s	9.9 $\pm$ 0.5	11.3 $\pm$ 0.8	10.8 $\pm$ 0.8

Values are means  $\pm$  SE. †*P* < 0.01 and \**P* < 0.05 vs. *Bin*<sub>0.1</sub> values by Tukey test. There were no significant differences in parameters between *Bin*<sub>0.3</sub> and *Bin*<sub>0.5</sub>.

Fig. 5. Effects of clonidine ( $1.5 \text{ mg} \cdot \text{kg}^{-1} \cdot \text{h}^{-1}$  iv) or medetomidine ( $1.5 \text{ mg} \cdot \text{kg}^{-1} \cdot \text{h}^{-1}$  iv) on the myocardial interstitial norepinephrine (NE) release in response to 5-Hz tonic cardiac sympathetic nerve stimulation. Data were obtained after sectioning vagal and cardiac sympathetic nerves. Clonidine administration does not affect baseline levels of NE (A), but significantly attenuates the stimulation-induced NE release (B). C: medetomidine administration does not affect baseline levels of NE. D: it does not attenuate the stimulation-induced NE release significantly. Values are means  $\pm$  SE. \* $P < 0.05$  from control.



response, the steady-state response was attenuated from  $-27.6 \pm 2.8$  to  $-12.2 \pm 0.7$  ( $P < 0.01$ ) and  $-6.7 \pm 0.4$  ( $P < 0.01$ ) ms during  $\text{Bin}_{0-3}$  and  $\text{Bin}_{0-5}$ , respectively. The initial slope was attenuated from  $-3.0 \pm 0.3$  to  $-1.1 \pm 0.1$  ( $P < 0.01$ ) and  $-0.65 \pm 0.06$  ( $P < 0.01$ ) ms/s during  $\text{Bin}_{0-3}$  and  $\text{Bin}_{0-5}$ , respectively.

Parameters of the transfer functions and step responses estimated in the supplemental protocol are summarized in Table 6. The steady-state gain of the transfer function and the steady-state response of the corresponding step response decreased with increase in the stimulus rate of the binary white noise sequence. Although the initial slope of the step response significantly decreased with increase in the stimulus rate of the binary white noise signal, the ratio of the steady-state response to the initial slope was unchanged. The natural frequency was lower and the damping coefficient was greater in  $\text{Bin}_{0-3}$  and  $\text{Bin}_{0-5}$  than  $\text{Bin}_{0-1}$  condition. The pure dead time of the transfer function did not differ among the three conditions.

Figure 5 summarizes the results of the supplemental protocol of NE measurement. Baseline levels of myocardial interstitial NE did not differ before and during clonidine administration (Fig. 5A). Clonidine administration attenuated the sympathetic stimulation-induced NE release to  $75.8 \pm 5.4\%$  of the control ( $P < 0.05$ ) (Fig. 5B). Baseline NE levels did not differ before and during medetomidine administration (Fig. 5C). Medetomidine did not attenuate the sympathetic stimulation-induced NE release significantly ( $92.0 \pm 6.7\%$  of the control, not significant) (Fig. 5D).

#### Simulation Study

To explore possible mechanisms for the observed differences between the presynaptic  $\alpha_2$ -adrenergic autoinhibition and the pharmacologic augmentation of the presynaptic inhibition via the

$\alpha_2$ -adrenergic receptors, we performed a simulation on the negative feedback regulation of the HR response to the sympathetic nerve stimulation. With reference to Fig. 6A,  $H_{FW}$  and  $H_{FB}$  represent the transfer functions of the forward path and the feedback path, respectively. A step input signal represents the sympathetic nerve stimulation. Both signals from presynaptic  $\alpha_2$ -adrenergic autoinhibition and pharmacologic augmentation of the presynaptic inhibition attenuate the input signal via the same  $\alpha_2$ -adrenergic receptors. Because the amount of neurotransmitter release cannot become negative, a threshold operator (Th) is added. The threshold operator is described mathematically as follows.

$$\text{Th}(x) = x \text{ when } x > 0, \text{ otherwise } \text{Th}(x) = 0$$

The output from the threshold operator or the amount of neurotransmitter is then fed into  $H_{FW}$  to yield the output or change in HR and is also fed into  $H_{FB}$  to yield the feedback signal of presynaptic  $\alpha_2$ -adrenergic autoinhibition. Since we administered clonidine  $\sim 15$  min before sympathetic nerve stimulation, the effect of clonidine should have reached steady state at the time of sympathetic nerve stimulation. Accordingly, we treated the pharmacologic augmentation of the presynaptic inhibition as a constant input. The magnitude of pharmacologic augmentation of the presynaptic inhibition was set arbitrarily to 0.5 to mimic the results of higher dose clonidine in protocol 2. The simulation was conducted using Matlab Simulink (The Mathworks, Natick, MA).

Yohimbine administration corresponds to severing the feedback path, i.e., setting  $H_{FB} = 0$  in the simulation. Under this condition, the transfer function from the input to output becomes  $H_{FW}$ . Therefore, we modeled  $H_{FW}$  using the second-order, low-pass filter with pure dead time (Eq. 3) with the

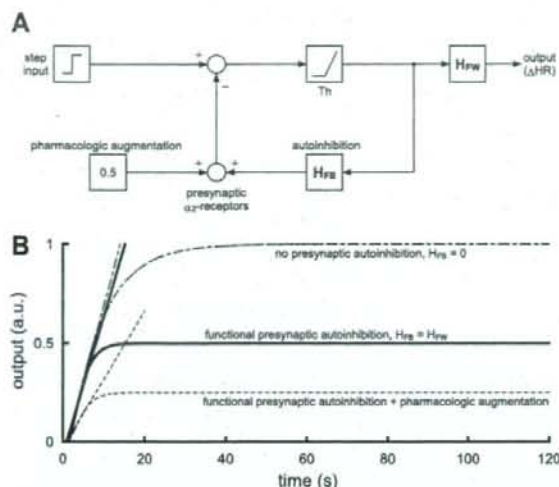


Fig. 6. Possible theoretical explanation for the differential effects of presynaptic  $\alpha_2$ -adrenergic autoinhibition and pharmacologic augmentation of presynaptic  $\alpha_2$ -adrenergic inhibition on the HR response to sympathetic nerve stimulation. *A*: a simulation model for the HR step response to a step input in the sympathetic nerve activity.  $H_{FW}$ , transfer function of the forward path;  $H_{FB}$ , transfer function of the feedback path;  $Th$ , a threshold operator (see main text for details). *B*: simulation results under conditions of no presynaptic inhibition (dash-dot line;  $H_{FB} = 0$  and pharmacologic augmentation of presynaptic inhibition = 0, corresponding to the yohimbine administration condition), functional presynaptic  $\alpha_2$ -adrenergic autoinhibition (solid line;  $H_{FB} = H_{FW}$  and pharmacologic augmentation of presynaptic inhibition = 0, corresponding to the control condition), and functional presynaptic  $\alpha_2$ -adrenergic autoinhibition plus pharmacologic augmentation of the presynaptic inhibition (dotted line;  $H_{FB} = H_{FW}$  and pharmacologic augmentation of presynaptic inhibition = 0.5, corresponding to the higher-dose clonidine condition). The presynaptic  $\alpha_2$ -adrenergic autoinhibition does not attenuate the initial slope of the step response. In contrast, the pharmacologic augmentation of the presynaptic inhibition attenuates the initial slope of the step response.

settings of  $f_N = 0.055$ ,  $\zeta = 1.55$ , and  $L = 0.94$  (Table 2, yohimbine). The gain was set at unity for simplicity. With this setting, we calculated the output response to the unit step input without the presynaptic inhibition (Fig. 6*B*, dash-dot line, corresponding to the yohimbine condition). The initial slope of the response, calculated from the linear regression analysis described in the method section, was 0.0763 arbitrary units (AU)/s. Next, we set  $H_{FB} = H_{FW}$  and performed a simulation of the condition with the presynaptic  $\alpha_2$ -adrenergic autoinhibition (Fig. 6*B*, solid line, corresponding to the control condition). The presynaptic  $\alpha_2$ -adrenergic autoinhibition attenuates the steady-state response without significantly affecting the initial slope of the response (0.0695 AU/s). Finally, we set the pharmacologic augmentation of the presynaptic inhibition to 0.5 on top of the functioning  $H_{FB}$ . The simulation result (Fig. 6*B*, dotted line, corresponding to the higher dose clonidine condition) demonstrates that pharmacologic augmentation of the presynaptic inhibition attenuates the steady-state response accompanied by a reduction in the initial slope of the response (0.0346 AU/s).

## DISCUSSION

We compared the blockade and activation of the presynaptic  $\alpha_2$ -adrenergic receptors and found a difference between the

presynaptic  $\alpha_2$ -adrenergic autoinhibition and the pharmacologic augmentation of the presynaptic inhibition in terms of HR response to sympathetic nerve stimulation. The presynaptic  $\alpha_2$ -adrenergic autoinhibition showed a limiter-like operation that restricts the steady-state response without affecting the initial slope of the response. In contrast, the pharmacologic augmentation of presynaptic inhibition showed an attenuator-like operation that reduces both the steady-state response and the initial slope of the response.

## Comparison of Blocking and Activating the Presynaptic $\alpha_2$ -Adrenergic Receptors

Although the presynaptic  $\alpha_2$ -adrenergic negative feedback has been known to attenuate the NE release and HR response to sympathetic nerve stimulation (9, 21, 26, 27, 29, 30, 31), the dynamic nature of the negative feedback remained to be elucidated. As shown in Fig. 2*C*, the blockade of  $\alpha_2$ -adrenergic receptors by yohimbine increased the steady-state response without significantly affecting the initial slope of the HR step response (Table 2). That is to say, the presynaptic  $\alpha_2$ -adrenergic autoinhibition of the presynaptic inhibition attenuates the steady-state response without sacrificing the rising speed of HR response to sympathetic nerve stimulation under control condition. These characteristics of the presynaptic  $\alpha_2$ -adrenergic autoinhibition conform to the limiter-like operation shown in Fig. 1*A*. In contrast, pharmacologic augmentation of the presynaptic inhibition by higher dose clonidine reduced the steady-state response accompanied by a decrease in the initial slope of the HR step response (Fig. 3*C*). The ratio of the steady-state response to the initial slope was not changed significantly by higher dose clonidine (Table 4), suggesting that attenuation of the initial slope was proportional to that of the steady-state response. These characteristics of the pharmacologic augmentation of the presynaptic inhibition conform to the attenuator-like operation shown in Fig. 1*B*. Rapid effector response is one of the most important hallmarks of neural regulation compared with humoral regulation. The findings of the present study suggest that presynaptic  $\alpha_2$ -adrenergic autoinhibition, but not pharmacologic augmentation of the presynaptic  $\alpha_2$ -adrenergic inhibition, prevents excess NE outflow at the sympathetic nerve terminals without compromising the rapidity of effector response. The simulation results suggest that the initial slope of the response decreases when presynaptic inhibition occurs, independent of the negative feedback mechanism (Fig. 6*B*). On the other hand, the initial slope of the response does not decrease significantly when the presynaptic inhibition occurs through the negative feedback mechanism.

$\alpha_2$ -Adrenergic receptors are classified as  $\alpha_{2A}$ ,  $\alpha_{2B}$ , and  $\alpha_{2C}$ -subtypes based on gene encodings (26). Furthermore, the different ligand binding characteristics of the  $\alpha_{2A}$ -subtype give rise to the pharmacological subtype of  $\alpha_{2A}$  in humans, rabbits, and pigs and that of  $\alpha_{2D}$  in rats, mice, and guinea pigs (26). The  $\alpha_{2A}$  and  $\alpha_{2D}$  may be considered as "orthologous"  $\alpha_2$ -receptors, with only one being present in any given species (27). In the sympathetic nerve,  $\alpha_{2A}$ - and  $\alpha_{2C}$ -receptors operate as presynaptic inhibitory autoreceptors, whereas  $\alpha_{2B}$ -receptors are located on postsynaptic cells to mediate the effects of catecholamine, such as vasoconstriction (26). In tissue slices from mouse atria,  $\alpha_{2A}$ -receptors inhibit NE release from sympathetic nerves primarily at high-stimulation rates (1–2 Hz), whereas

$\alpha_{2C}$ -receptors can operate at very low stimulation rates (0.05–0.1 Hz) (10). Because  $\alpha_{2A}$ -receptors in the rabbit heart are characterized as  $\alpha_{2A}$ , changes in the transfer function from sympathetic nerve stimulation to HR response observed in the present study are most likely mediated by  $\alpha_{2A}$ -receptors.

Clonidine administration (5  $\mu\text{g}/\text{kg}$  bolus followed by 30  $\mu\text{g}\cdot\text{kg}^{-1}\cdot\text{h}^{-1}$  iv) attenuated the sympathetic outflow from the central nervous system in rabbits (35). However, lower dose clonidine at 0.3  $\text{mg}\cdot\text{kg}^{-1}\cdot\text{h}^{-1}$  failed to significantly affect the steady-state response or the initial slope of the HR step response in the present study (Fig. 3B, Table 4), suggesting a difference in clonidine sensitivity between the central and peripheral sympathetic nervous systems. Another factor that should be taken into account is the operating range of the HR control (i.e., mean HR during dynamic sympathetic stimulation). As an example, tonic vagal stimulation decreased mean HR during dynamic sympathetic stimulation, which increased the dynamic gain of sympathetic HR control via nonlinear sigmoidal input-output nature between autonomic activities and HR (12, 13). Therefore, the decrease in the mean HR during lower dose clonidine, although it was statistically insignificant (Table 3), should have an effect of increasing the dynamic gain of the sympathetic HR control. Such an effect might have counterbalanced the effect of reducing the dynamic gain via presynaptic inhibition during the lower dose clonidine administration. Although higher dose clonidine decreased mean HR before and during sympathetic nerve stimulation, mean AP did not decrease compared with lower dose clonidine (Table 3). The discrepancy between the changes in mean HR and AP may be due to direct vasoconstriction by higher dose clonidine through  $\alpha$ -adrenergic stimulation.

#### Transfer Function Analysis vs. Step Response Analysis

In a previous study, our laboratory performed a transfer function analysis on the sympathetic HR control using a binary white noise signal (12, 23). The transfer function is a frequency-domain representation of the system dynamic characteristics over a wide frequency range and is useful for understanding the behavior of the system in response to a variety of input signals (3, 7, 21). Notwithstanding the theoretical advantages of the

transfer function, the frequency-domain representation may be somewhat unfamiliar to most physiologists. Therefore, we calculated the step responses corresponding to the transfer functions. As can be seen in Figs. 2, B and C and 3, B and C, changes in transfer function in the lower frequency range reflect the steady-state response in the step response. Changes in transfer function in the higher frequency range reflect the initial transient response in the step response. Because the step response and the transfer function are mathematically interchangeable, both the transfer function and the step response provide comparable information on the system dynamic characteristics.

In a previous study, our laboratory has shown that increasing mean stimulus rate of the Gaussian white noise decreased the steady-state gain of the transfer function from sympathetic nerve stimulation to HR without affecting the natural frequency or damping coefficient significantly (23). Increasing the stimulus rate of the binary white noise signal also caused an approximately parallel downward shift in the gain plot (Fig. 4B). The transfer function parameters, however, showed a decrease in the natural frequency and an increase in the damping coefficient (Table 6). The higher natural frequency in Bin<sub>0.1</sub> than in Bin<sub>0.5</sub> condition may account for the higher natural frequency in *protocol 1* (Bin<sub>0.1</sub> was used for sympathetic stimulation) than in *protocol 2* (Bin<sub>0.5</sub> was used for sympathetic stimulation) observed under control conditions. Notwithstanding the differences in the natural frequency and the damping coefficient, the ratio of the step response to the initial slope was not changed significantly by the difference in the stimulus rate of the binary white noise signal. Therefore, yohimbine-induced changes in the ratio of the step response to the initial slope observed in *protocol 1* (Table 1) cannot be explained by changes in the magnitude of sympathetic effect on HR.

#### Limitations

The present study has several limitations. First, we performed the experiment under anesthetic conditions. However, because we compared the effects of yohimbine and clonidine on the sympathetic HR control under the same anesthetic

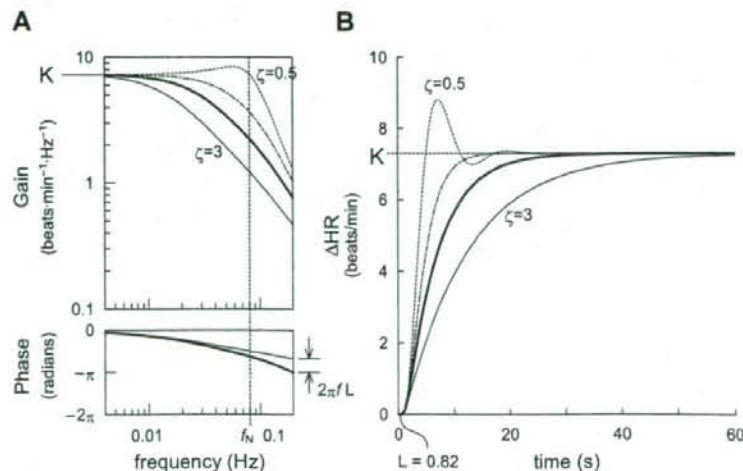


Fig. 7. Schematic explanation for the frequency response of a second-order, low-pass filter with pure dead time ( $L$ ; A), and the corresponding step response (B).  $K$ , dynamic gain;  $f_n$ , natural frequency;  $\zeta$ , damping ratio. See APPENDIX for details.



condition, the interpretation of the observed changes in the transfer function may be reasonable. Second, the simulation model in Fig. 6A is not the only model that can be applied to the observed results. Although the model is convenient to explain many aspects of the observed results, other models may also be applicable to the present observation. Third, clonidine can affect HR through non- $\alpha_2$ -adrenergic mechanisms. For instance, clonidine caused bradycardia in  $\alpha_2$ ABC-knockout mouse via direct inhibition of cardiac hyperpolarization-activated cyclic nucleotide-gated pacemaker channels (16). While we tried to use medetomidine instead of clonidine, medetomidine did not attenuate myocardial interstitial NE release in response to sympathetic nerve stimulation significantly, at least, at the same dose as clonidine (Fig. 5). Further studies using other agonists might be required to confirm our observations. Finally, we used a weak stimulus rate (0 to 1 Hz) for the yohimbine protocol. Although we had examined the effect of yohimbine using a strong stimulus rate (0–5 Hz) in a preliminary study, the steady-state gain of the transfer function did not increase much ( $8.4 \pm 1.7$  vs.  $9.0 \pm 1.7$  beats  $\cdot$  min $^{-1}$   $\cdot$  Hz $^{-1}$ ,  $n = 3$ ). Under such strong stimulus condition, the saturation of HR response might have masked the effect of presynaptic inhibition. Therefore, the result of protocol 1 should be carefully interpreted in view of the existence of a stimulus rate-drug interaction effect.

### Conclusions

The presynaptic  $\alpha_2$ -adrenergic autoinhibition attenuates the dynamic HR response to sympathetic nerve stimulation in the low-frequency range (0.004–0.04 Hz) but not in the high-frequency range (0.05–0.15 Hz). In the time domain, the presynaptic  $\alpha_2$ -adrenergic autoinhibition attenuates the steady-state response without affecting the slope of the response in the HR step response (a limiter-like operation). In contrast, pharmacologic augmentation of presynaptic  $\alpha_2$ -adrenergic inhibition attenuates the dynamic HR response to sympathetic nerve stimulation in a frequency-independent manner. In the time domain, pharmacologic augmentation of the presynaptic inhibition attenuates not only the steady-state response but also the initial slope of the HR step response (an attenuator-like operation). Presynaptic  $\alpha_2$ -adrenergic autoinhibition would be favorable for limiting excess NE outflow at the sympathetic nerve terminals without compromising the rapidity of effector response.

### APPENDIX

#### Mathematical Modeling of the Sympathetic HR Response

To describe the estimated transfer function, we used a second-order, low-pass filter with pure dead time ( $L$ ). Figure 7A shows the frequency response of a second-order, low-pass filter with  $L$ . Figure 7B shows the corresponding step response. The step response is calculated for 1-Hz sympathetic nerve stimulation. The steady-state gain ( $K$ ) of the transfer function represents the value of transfer gain as the frequency approaches zero. The  $K$  corresponds to the steady-state response in the step-response representation. The natural frequency ( $f_N$ ) determines the upper frequency limit of the low-pass filter. For instance, if the  $f_N$  were 10 times higher, the frequency axis in Fig. 7A would have to be scaled by a factor of 10, indicating that the system could respond to 10-fold higher frequency input. The phase plot in Fig. 7A indicates that, at the  $f_N$ , the output is delayed by  $\pi/2$  radians relative to the input, in the absence of the  $L$ . The maximum

phase delay of the second-order, low-pass filter is  $\pi$  radians in the absence of  $L$ . The  $L$  is needed to account for the phase difference between the estimated transfer function and the second-order, low-pass filter. In Fig. 7B, the  $L$  corresponds to the time difference between the onset of the step input and the onset of the response. The damping coefficient ( $\zeta$ ) characterizes the system response around the  $f_N$ . As an example, the gain plot shows a slight peak around  $f_N$  when  $\zeta = 0.5$  (dotted line). Figure 7B shows that a  $\zeta$  of 0.5 causes an initial overshoot in response to a step change in the input. A system with  $\zeta < 1$  is called underdamped. On the other hand, the gain plot shows more gradual decrease around  $f_N$  when  $\zeta = 3$  (fine solid line). Figure 7B shows that the system responds sluggishly when  $\zeta = 3$ . A system with  $\zeta > 1$  is called overdamped. A system with  $\zeta = 1$  is called critically damped (dash-dot line). The  $\zeta$  of the estimated transfer functions ranged from 1.55 to 1.72 in the present study, indicating that the sympathetic HR control system is overdamped. The solid line represents the second-order, low-pass filter with  $\zeta = 1.64$  and  $L = 0.82$  that is derived from the mean value obtained under control condition in protocol 1.

### GRANTS

This study was supported by "Health and Labour Sciences Research Grant for Research on Advanced Medical Technology," "Health and Labour Sciences Research Grant for Research on Medical Devices for Analyzing, Supporting and Substituting the Function of Human Body," and "Health and Labour Sciences Research Grant H18-Iryo-Ippan-023" from the Ministry of Health, Labour and Welfare of Japan; "Program for Promotion of Fundamental Studies in Health Science" from the National Institute of Biomedical Innovation; and "Ground-based Research Announcement for Space Utilization" promoted by the Japan Space Forum.

### REFERENCES

- Altman JD, Trendelenburg AU, MacMillan L, Bernstein D, Limbird L, Starke K, Kobilka BK, Hein L. Abnormal regulation of the sympathetic nervous system in  $\alpha_2$ -adrenergic receptor knockout mice. *Mol Pharmacol* 56: 154–161, 1999.
- Bendat JS, Piersol AG. Single-input/output relationships. In: *Random Data Analysis and Measurement Procedures* (3rd Ed.). New York: Wiley, 2000, p. 189–217.
- Berger RD, Saul JP, Cohen RJ. Transfer function analysis of autonomic regulation. I. Canine atrial rate response. *Am J Physiol Heart Circ Physiol* 256: H142–H152, 1989.
- Brigham EO. FFT transform applications. In: *The Fast Fourier Transform and Its Applications*. Englewood Cliffs, NJ: Prentice-Hall, 1988, p. 167–203.
- Buhler FR, Bolli P, Amann WF, Erne P, Kiowski W. Sympathetic nervous system in essential hypertension and antihypertensive response to  $\alpha_2$ -adrenoceptor stimulation. *J Cardiovasc Pharmacol* 6: S753–S756, 1984.
- Franklin GF, Powell JD, and Emani-Naeini A. Dynamic models and dynamic response. In: *Feedback Control of Dynamic Systems* (2nd Ed.). Boston, MA: Addison-Wesley, 1991, p. 17–144.
- Glantz SA. *Primer of Biostatistics* (5th Ed.). New York: McGraw-Hill, 2002.
- Grossman E, Chang PC, Hoffman A, Tamrat M, Goldstein DS. Evidence for functional  $\alpha_2$ -adrenoceptors on vascular sympathetic nerve endings in the human forearm. *Circ Res* 69: 887–897, 1991.
- Hein L, Altman JD, Kobilka BK. Two functionally distinct  $\alpha_2$ -adrenergic receptors regulate sympathetic neurotransmission. *Nature* 402: 181–184, 1999.
- Jie K, van Brummelen P, Vermeij P, Timmermans PB, van Zwieten PA. Modulation of noradrenaline release by peripheral presynaptic  $\alpha_2$ -adrenoceptors in humans. *J Cardiovasc Pharmacol* 9: 407–413, 1987.
- Kawada T, Ikeda Y, Sugimachi M, Shishido T, Kawaguchi O, Yamazaki T, Alexander J Jr, Sunagawa K. Bidirectional augmentation of heart rate regulation by autonomic nervous system in rabbits. *Am J Physiol Heart Circ Physiol* 271: H288–H295, 1996.
- Kawada T, Sugimachi M, Shishido T, Miyano H, Sato T, Yoshimura R, Miyashita H, Nakahara T, Alexander J Jr, Sunagawa K. Simultaneous identification of static and dynamic vagosympathetic interactions in regulating heart rate. *Am J Physiol Regul Integr Comp Physiol* 276: R782–R789, 1999.

14. Kawada T, Yamazaki T, Akiyama T, Sato T, Shishido T, Sugimachi M, Inagaki M, Alexander J Jr, Sunagawa K. Liquid chromatographic determination of myocardial interstitial epinephrine. *J Chromatogr B Biomed Sci Appl* 714: 375-378, 1998.
15. Kawada T, Yamazaki T, Akiyama T, Sato T, Shishido T, Yoshimura R, Inagaki M, Tatewaki T, Sugimachi M, Sunagawa K. Local epinephrine release in the rabbit myocardial interstitium in vivo. *J Auton Nerv Syst* 78: 94-98, 2000.
16. Knaus A, Zong X, Beetz N, Jahns R, Lohse MJ, Biel M, Hein L. Direct inhibition of cardiac hyperpolarization-activated cyclic nucleotide-gated pacemaker channels by clonidine. *Circulation* 115: 872-880, 2007.
17. Langer SZ. 25 years since the discovery of presynaptic receptors, present knowledge and future perspectives. *Trends Pharmacol Sci* 18: 95-99, 1997.
18. Langer SZ. Presence and physiological role of presynaptic inhibitory  $\alpha_2$ -adrenoceptors in guinea pig atria. *Nature* 294: 671-672, 1981.
19. Langer SZ, Adler-Graschinsky E, Giorgi O. Physiological significance of  $\alpha$ -adrenoceptor-mediated negative feedback mechanism regulating noradrenaline release during nerve stimulation. *Nature* 265: 648-650, 1977.
20. Langer SZ. Presynaptic regulation of catecholamine release. *Biochem Pharmacol* 23: 1793-1800, 1974.
21. Marmarelis PZ, Marmarelis VZ. The white noise method in system identification. In: *Analysis of Physiological Systems*. New York: Plenum, 1978, p. 131-221.
22. Miyamoto T, Kawada T, Yanagiya Y, Takaki H, Inagaki M, Sugimachi M, Sunagawa K. Cardiac sympathetic nerve stimulation does not attenuate dynamic vagal control of heart rate via  $\alpha$ -adrenergic mechanism. *Am J Physiol Heart Circ Physiol* 287: H860-H865, 2004.
23. Nakahara T, Kawada T, Sugimachi M, Miyano H, Sato T, Shishido T, Yoshimura R, Miyashita H, Inagaki M, Alexander J Jr, Sunagawa K. Neuronal uptake affects dynamic characteristics of heart rate response to sympathetic stimulation. *Am J Physiol Regul Integr Comp Physiol* 277: R140-R146, 1999.
24. Niederhoffer N, Hein L, Starke K. Modulation of the baroreceptor reflex by  $\alpha_{2A}$ -adrenoceptors, a study in  $\alpha_{2A}$  knockout mice. *Br J Pharmacol* 141: 851-859, 2004.
25. Pelayo F, Dubocovich ML, Langer SZ. Regulation of noradrenaline release in the rat pineal through a negative feedback mechanism mediated by presynaptic  $\alpha$ -adrenoceptors. *Eur J Pharmacol* 45: 317-318, 1977.
26. Philipp M, Brede M, Hein L. Physiological significance of  $\alpha_2$ -adrenergic receptor subtype diversity, one receptor is not enough. *Am J Physiol Regul Integr Comp Physiol* 283: R287-R295, 2002.
27. Rump LC, Bohmann C, Schaible U, Schöllhorn J, Limberger N.  $\alpha_2C$ -Adrenoceptor-modulated release of noradrenaline in human right atrium. *Br J Pharmacol* 116: 2617-2624, 1995.
- 27a. Schwartz DD. Activation of  $\alpha_2$  adrenergic receptors inhibits norepinephrine release by a pertussis toxin-insensitive pathway independent of changes in cytosolic calcium in cultured rat sympathetic neurons. *J Pharmacol Exp Ther* 282: 248-255, 1997.
28. Sinclair MD. A review of the physiological effects of  $\alpha_2$ -agonists related to the clinical use of medetomidine in small animal practice. *Can Vet J* 44: 885-897, 2003.
29. Starke KM, Gothert M, Kilbinger H. Modulation of neurotransmitter release by presynaptic autoreceptors. *Physiol Rev* 69: 864-989, 1989.
30. Starke KM. Presynaptic  $\alpha$ -autoreceptors. *Rev Physiol Biochem Pharmacol* 107: 73-146, 1987.
31. Starke K, Langer SZ. A note on terminology for presynaptic receptors. In: *Presynaptic Receptors*, edited by Langer SZ, Starke K, and Dubocovich ML. Oxford, UK: Pergamon 1979, p. 1-3.
32. Starke K, Endo T, Taube HD. Pre- and post-synaptic components in effect of drugs with  $\alpha$ -adrenoceptor affinity. *Nature* 254: 440-441, 1975.
33. Starke K. Alpha sympathomimetic inhibition of adrenergic and cholinergic transmission in the rabbit heart. *Naunyn-Schmiedeberg's Arch Pharmacol* 274: 18-45, 1972.
34. Szabo B, Schramm A, Starke K. Effect of yohimbine on renal sympathetic nerve activity and renal norepinephrine spillover in anesthetized rabbits. *J Pharmacol Exp Ther* 260: 780-788, 1992.
35. Szabo B, Hedler L, Starke K. Peripheral presynaptic and central effects of clonidine, yohimbine and rauwolfscine on the sympathetic nervous system in rabbits. *Naunyn-Schmiedeberg's Arch Pharmacol* 340: 648-657, 1989.
37. Vizi ES, Somogyi GT, Hadhazy P, Knoll J. Effect of duration and frequency of stimulation on the presynaptic inhibition by  $\alpha$ -adrenoceptor stimulation of the adrenergic transmission. *Naunyn-Schmiedeberg's Arch Pharmacol* 280: 79-91, 1973.
38. Westfall TC. Local regulation of adrenergic neurotransmission. *Physiol Rev* 57: 659-728, 1977.



## Vagal stimulation suppresses ischemia-induced myocardial interstitial myoglobin release

Toru Kawada<sup>a,\*</sup>, Toji Yamazaki<sup>b</sup>, Tsuyoshi Akiyama<sup>b</sup>, Hirotohi Kitagawa<sup>c</sup>, Shuji Shimizu<sup>a</sup>, Masaki Mizuno<sup>a</sup>, Meihua Li<sup>a</sup>, Masaru Sugimachi<sup>a</sup>

<sup>a</sup> Department of Cardiovascular Dynamics, Advanced Medical Engineering Center, National Cardiovascular Center Research Institute, Osaka 565-8565, Japan

<sup>b</sup> Department of Cardiac Physiology, National Cardiovascular Center Research Institute, Osaka 565-8565, Japan

<sup>c</sup> Department of Anesthesiology, Shiga University of Medical Science, Shiga 520-2192, Japan

### ARTICLE INFO

#### Article history:

Received 19 May 2008

Accepted 23 July 2008

#### Keywords:

Coronary artery occlusion

Cardiac microdialysis

Cats

### ABSTRACT

**Aims:** To evaluate vagal stimulation-mediated myocardial protection against ischemia and reperfusion in *in vivo* ischemic myocardium.

**Main methods:** We measured myocardial interstitial myoglobin levels in the ischemic region using a cardiac microdialysis technique in anesthetized and vagotomized cats. We occluded the left anterior descending coronary artery (LAD) for 60 min and reperused it for 60 min (VX group,  $n=6$ ). The effects of bilateral vagal stimulation (10 V, 5 Hz, 1-ms pulse duration), initiated immediately after LAD occlusion, were examined (VS group,  $n=6$ ). To examine the involvement of phosphatidylinositol 3-kinase (PI3K), vagal stimulation was performed after pretreatment with a PI3K inhibitor wortmannin (0.6 mg/kg, *i.v.*) (VS-W group,  $n=6$ ). To examine the contribution of bradycardia, vagal stimulation was performed with fixed-rate ventricular pacing (VS-P group,  $n=6$ ).

**Key findings:** The average myoglobin level during the ischemic period was  $1170 \pm 141$  in VX (in ng/ml, mean  $\pm$  SE), which was significantly attenuated in VS ( $466 \pm 87$ ,  $P < 0.05$ ) and VS-W ( $613 \pm 124$ ,  $P < 0.05$ ) but not in VS-P ( $953 \pm 203$ ). Reperfusion increased the myoglobin level to  $2500 \pm 544$  in VX, whereas it was suppressed in VS ( $824 \pm 213$ ,  $P < 0.05$ ) and VS-W ( $948 \pm 315$ ,  $P < 0.05$ ) but not in VS-P ( $1710 \pm 253$ ).

**Significance:** Vagal stimulation, initiated immediately after LAD occlusion, attenuated the myocardial injury. Moreover, bradycardia, independent of PI3K pathway, plays a significant role in vagally induced cardioprotection during acute myocardial ischemia.

© 2008 Elsevier Inc. All rights reserved.

### Introduction

An increase in parasympathetic tone can provide cardioprotection against acute myocardial ischemia and infarction via the direct effects of acetylcholine (ACh) on the ischemic myocardium and the indirect effects mediated by altered hemodynamics. For the direct effects, administration of ACh prior to a coronary artery occlusion reduces the infarct size in isolated, perfused rabbit heart (Qin et al., 2003). Phosphatidylinositol 3-kinase (PI3K) is thought to be an upstream enzyme in the signal transduction pathway for the ACh-induced, ischemic preconditioning mimetic effect (Qin et al., 2003; Oldenburg et al., 2003). For the indirect effects, vagal stimulation reduces myocardial oxygen consumption due to bradycardia (Sammel et al., 1983) and also decreases ventricular contractility via antagonism of the sympathetic effect (Nakayama et al., 2001). Vagal stimulation can also dilate the coronary artery (Feigl, 1969; Reid et al., 1985; Feliciano and Henning, 1998; Henning and Sawmiller, 2001), which may increase collateral flow into the ischemic region.

In a previous study, we demonstrated that efferent vagal stimulation nearly halved the increase in myocardial interstitial norepinephrine levels in the ischemic region of the feline ventricle (Kawada et al., 2006). Whether vagal stimulation can reduce myocardial damage in the ischemic region, however, has yet to be directly examined. To test the hypothesis that vagal stimulation reduces myocardial injury in the ischemic region, we measured myocardial interstitial myoglobin levels during acute myocardial ischemia and reperfusion with or without efferent vagal stimulation in anesthetized cats. We examined possible involvement of the PI3K signaling pathway using vagal stimulation and pretreatment with a PI3K inhibitor wortmannin. We also examined the contribution of bradycardia using vagal stimulation and fixed-rate ventricular pacing.

### Materials and methods

#### Surgical preparation

Animal care was provided in strict accordance with the *Guiding Principles for the Care and Use of Animals in the Field of Physiological Sciences* approved by the Physiological Society of Japan. Adult cats

\* Corresponding author. Department of Cardiovascular Dynamics, National Cardiovascular Center Research Institute, 5-7-1 Fujishirodai, Suita, Osaka 565-8565, Japan. Tel.: +81 6 6833 5012x2427; fax: +81 6 6835 5403.

E-mail address: [torukawa@res.nccv.go.jp](mailto:torukawa@res.nccv.go.jp) (T. Kawada).

weighing between 2.3 and 4.2 kg were anesthetized with an intraperitoneal injection of pentobarbital sodium (30–35 mg/kg) and ventilated mechanically with room air mixed with oxygen. The depth of anesthesia was maintained with a continuous intravenous infusion of pentobarbital sodium ( $1-2 \text{ mg kg}^{-1} \text{ h}^{-1}$ ) through a catheter inserted into the right femoral vein. Systemic arterial pressure (AP) was monitored from a catheter inserted into the right femoral artery. The heart rate (HR) was determined from an electrocardiogram using a cardiostimulator. The esophageal temperature of the animal was measured using a thermometer (CTM-303, TERUMO, Japan) and was maintained at approximately  $37^\circ\text{C}$  using a heated pad and a lamp.

Bilateral vagal nerves were exposed and sectioned through a midline cervical incision. With the animal in the lateral position, the left fifth and sixth ribs were resected to allow access to the heart. The heart was suspended in a pericardial cradle. Using a fine guiding needle, a dialysis probe was implanted into the anterolateral free wall of the left ventricle perfused by the left anterior descending coronary artery (LAD) (Akiyama et al., 1994). A 3-0 silk suture was passed around the LAD just distal to the first diagonal branch for subsequent coronary occlusion. For bilateral vagal stimulation, a pair of bipolar platinum electrodes was attached to the cardiac end of each sectioned vagal nerve. The nerves and electrodes were covered with warmed mineral oil for insulation. Heparin sodium (100 U/kg) was administered intravenously to prevent blood coagulation. At the end of the experiment, the animals were killed with an overdose of intravenous pentobarbital sodium. We confirmed that the semipermeable membrane of the dialysis probe had been implanted within the left ventricular myocardium.

#### Dialysis technique

The materials and properties of the transverse dialysis probe have been previously described (Kitagawa et al., 2005). Briefly, both ends of a dialysis fiber (length, 8 mm; outer diameter, 215  $\mu\text{m}$ ; inner diameter, 175  $\mu\text{m}$ ; pore size, 300  $\text{\AA}$ ; Evaflux type 5A, Kuraray Medical, Japan) were glued to polyethylene tubes (length, 25 cm; outer diameter, 500  $\mu\text{m}$ ; inner diameter, 200  $\mu\text{m}$ ). The dialysis probe was perfused with Ringer's solution at the rate of 5  $\mu\text{l}/\text{min}$  using a microinfusion pump (CMA/100, Carnegie Medicine). Dialysate sampling was initiated 2 h after implanting the dialysis probe, at which point the concentration of myoglobin in the dialysate had reached a steady state (Kitagawa et al., 2005). The actual dialysate sampling period lagged behind a given collection period by 2 min due to the dead space volume between the dialysis membrane and the sample tube. The concentration of myoglobin in the dialysate was measured immunochemically (Cardiac Reader, Roche Diagnostics). The detection limit for myoglobin was 30 ng/ml. The sample was diluted in Ringer's solution whenever necessary and the concentration was corrected for the dilution factor.

#### Protocols

##### Protocol 1 (VX group, $n=6$ )

As a control group, we measured changes in the myocardial interstitial myoglobin levels of vagotomized cats subjected to 60 min of LAD occlusion followed by 60 min of reperfusion. After collecting a 15-min baseline dialysate sample, we occluded the LAD for 60 min and collected four consecutive 15-min dialysate samples during the ischemic period. We then released the occlusion and collected additional four consecutive 15-min dialysate samples during the 60-min reperfusion period.

##### Protocol 2 (VS group, $n=6$ )

We examined the effects of bilateral vagal stimulation on the release of myocardial interstitial myoglobin. To avoid the potential preconditioning mimetic effects of ACh released in response to the vagal stimulation (Kawada et al., 2002; Przyklenk and Kloner, 1995), we initiated bilateral vagal stimulation (5 Hz, 10 V, 1-ms pulse

duration) immediately after the LAD occlusion and continued it throughout the 60-min ischemic period and the 60-min reperfusion period. Dialysate samples were collected in the same manner described for Protocol 1.

##### Protocol 3 (VS-W group, $n=6$ )

Because PI3K is involved in the direct cardioprotective effects of ACh (Qin et al., 2003; Oldenburg et al., 2003), we examined the contribution of PI3K to the effects of vagal stimulation on ischemia-induced myocardial injury. A PI3K inhibitor wortmannin was administered (0.6 mg/kg i.v. bolus) 15 min before the onset of the baseline dialysate sampling. After collecting the baseline dialysate sample, LAD occlusion and reperfusion were each performed for 60 min. Bilateral vagal stimulation was started immediately after the LAD occlusion and was continued until the end of the reperfusion period. Dialysate samples were collected as described in Protocol 1.

##### Protocol 4 (VS-P group, $n=6$ )

Because bradycardia is a major hemodynamic change induced by vagal stimulation, we examined the contribution of bradycardia to the effects of vagal stimulation on ischemia-induced myocardial injury. After collecting the baseline dialysate sample, LAD occlusion and reperfusion were each performed for 60 min. Bilateral vagal stimulation and fixed-rate ventricular pacing (200 beats/min) were both started immediately after the LAD occlusion and were continued throughout the ischemic and reperfusion periods. Dialysate samples were collected as described in Protocol 1.

#### Statistical analysis

All data are presented as the means and SE. To examine the effects of coronary occlusion and reperfusion on the myocardial interstitial myoglobin levels in each group, we compared the myoglobin levels during the ischemic and reperfusion periods with the baseline level (eight comparisons) and the myoglobin levels during the reperfusion period with the myoglobin level during the last 15 min of ischemia (four comparisons) using Holm's *t* test for 12 comparisons (Glantz, 2002). Briefly, after calculating *P* values for the 12 comparisons using paired-*t* test, the *P* values were sorted based on their size. The smallest *P* value was multiplied by 12 (the number of total comparisons), the next smallest *P* value was multiplied by 11 (the number of total comparisons minus 1), and so on. The Holm's test is less conservative than the ordinary Bonferroni method. Because the myoglobin level changed by more than an order of magnitude, comparisons were made after a logarithmic conversion. Differences were considered significant at  $P<0.05$ .

To compare myoglobin levels among the VX, VS, VS-W and VS-P groups, we used one-way ANOVA (analysis of variance). When there were significant differences among the groups, Dunnett's test was applied to examine the differences between the VS, VS-W, or VS-P group and the VX group (Glantz, 2002). The myoglobin levels at different time points as well as averaged myoglobin levels during the ischemic period, reperfusion period, and total period throughout ischemia and reperfusion were compared. Differences were considered significant at  $P<0.05$ .

HR and mean AP were measured immediately before the LAD occlusion (denoted as time 0), at 15, 30, 45 and 60 min of ischemia and at 15, 30, 45 and 60 min of reperfusion. The data for the HR and mean AP were compared among the VX, VS, VS-W, and VS-P groups using one-way ANOVA followed by Dunnett's test with the VX group value as the control. Differences were considered significant at  $P<0.05$ .

#### Results

Changes in the myocardial interstitial myoglobin levels are summarized in Fig. 1. In the VX group, the LAD occlusion significantly